THE JOURNAL
OF
CHEMICAL PHYSICS

VOLUME 13, NUMBER 8 AUGUST, 1945

The Near Ultraviolet Absorption Spectrum of Phenol Vapor

F. A. MATSEN
Department of Chemistry,

NATHAN GINSBURG AND W. W. ROBERTSON
Department of Physics, The University of Texas, Austin, Texas

(Received April 20, 1945)

The absorption spectrum of phenol as observed with a 3-m grating spectrograph consisted of 330 bands. A tentative analysis is made on the basis of the fundamental ground-state frequencies 245, 397, 527, 811, 824, and 999 and the fundamental excited-state frequencies 208, 374, 476, 562, 783, 935, 975, 1274, and 1565. These agree well with Raman data.

INTRODUCTION

THE substitution of the OH group on the benzene ring modifies the electronic structure of the ring by an inductive effect and by a resonance effect involving the unshared pairs of electrons on the oxygen atom. This results in an intensification of the spectrum and an increase in the number of allowed vibrational transitions over that of benzene similar to the situation found in aniline[1] and chlorobenzene.[2] The absorbing power of phenol has been estimated to be 230 times that of benzene.[3]

The ultraviolet absorption spectrum of phenol has been investigated by Savard,[4] Masaki,[5] Asagoe, Shimokawa, and Kageyama,[3] and by Hall.[6] These investigators have not presented the complete spectrum nor have they presumably resolved the doublet fine structure of phenol. Savard analyzed 120 bands on the basis of four frequencies. However, he assumed the vibrational frequencies to be the same in the excited state as in the ground state which invalidated his assignment, and further, he did not make correlation with Raman data. Neither Masaki nor Hall give any detailed analysis. Asagoe, Shimokawa, and Kageyama made an analysis on the basis of five fundamental frequencies in the excited state and two in the ground state.

The Raman spectrum has been studied by Kahovec and Reitz,[7] Masaki,[5] and Kohlrausch and Wittek.[8]

EXPERIMENTAL

The absorption spectrum of phenol was studied in the first order of a spectrograph of the Eagle type, with a 3-meter grating ruled 15,000 lines per inch, to determine the optimum conditions. A series of plates were taken in the second order at temperatures of the absorption call ranging from 24°C to 120°C while the temperature of the

[1] N. Ginsburg and F. A. Matsen, J. Chem. Phys. **13**, 167 (1945).
[2] H. Sponer and S. H. Wollman, J. Chem. Phys. **9**, 816 (1941).
[3] K. Asagoe, Y. Shimokawa, and S. Kageyama, Jap. J. Phys. **14**, 11 (1940).
[4] J. Savard, Ann. de Chim. **11**, 287 (1929).
[5] K. Masaki, Bull. Chem. Soc. Japan **11**, 346 (1936).
[6] M. B. Hall, Phys. Rev. **61**, 736 (A) (1942).
[7] L. Kahovec and A. W. Reitz, Monatsh. **69**, 363 (1936).
[8] K. W. F. Kohlrausch and H. Wittek, Monatsh. **74**, 1 (1943).

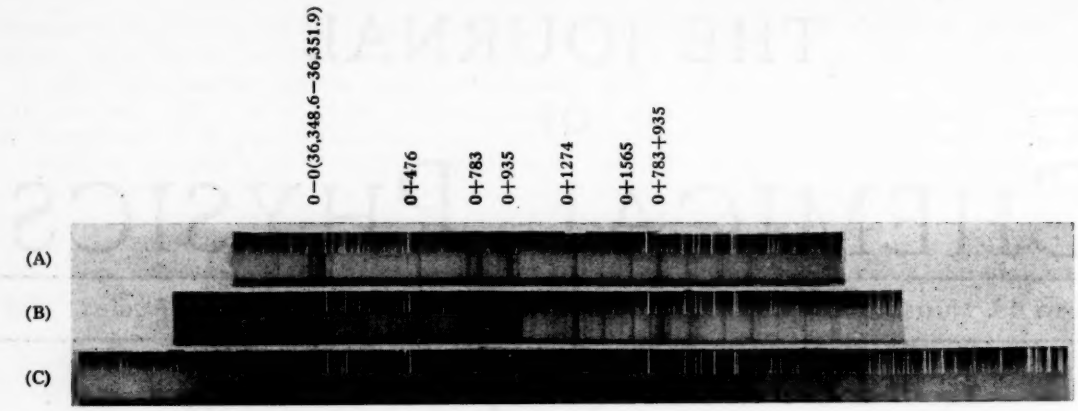

FIG. 1. Pressure development of the phenol spectrum. Cell temperature 24°C; reservoir temperatures: (*A*) −37°C, (*B*) 0°C, and (*C*) 24°C.

phenol reservoir, which controlled the pressure, was varied between −37°C and 90°C. The accompanying figure (Fig. 1) illustrates the development of the spectrum.

The plates used were Eastman Kodak 103–0. The phenol, "Special Absolute Pure" Phenol C. P., prepared by the National Aniline and Chemical Company, was redistilled under vacuum. The absorption cell, as all quartz, was 70 cm long. The light source was a 500 volt 2.5 kva hydrogen discharge tube, sufficiently powerful to give exposures in two hours even with the use of the necessary filters.

No photo-decomposition was observed for phenol. The absorption cell was pumped out and refilled several times during the course of the investigation, but there was no noticeable decrease in the intensity of the exposure durings several runs.

Over 300 bands were observed in the spectrum in the region 2490–2830A. Table I gives the wave-length, wave number, intensity, and assignment of these bands. Since many of the bands appear as very sharp doublets, measurements were made to the centers of absorption in these cases, and the method was carried over to the broad, more diffuse bands. For the doublets, the precision was estimated to be 0.3 cm^{-1}, with the accuracy diminishing to 2 cm^{-1} for the weak, diffuse bands. In the table, all doublets are grouped in pairs. In making intensity assignments, allowance was made for the effect of varying pressures.

In the spectrum of phenol some seventy doublets were found with a mean separation of three wave numbers. This doublet character for a number of bands was found to depend on the temperature and pressure of the phenol. Some doublets were found only at high temperatures and pressures; others, which were broad and diffuse at both low and high temperatures and pressures, were doublets at intermediate values. Almost without exception, however, the identifiable fundamental frequencies produced persistent doublet bands.

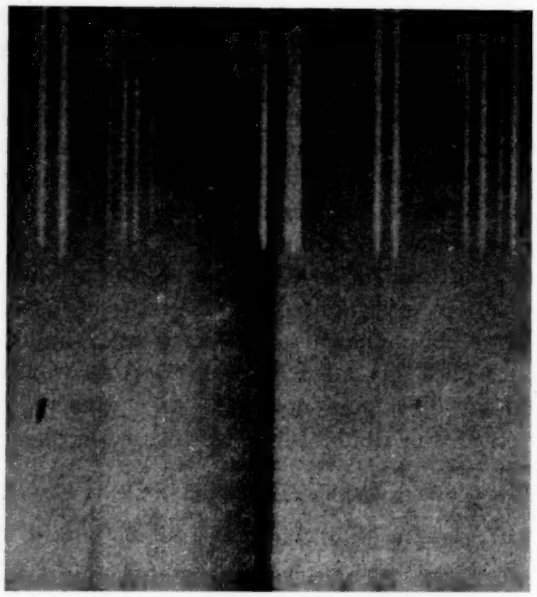

FIG. 2. Enlargement (×12) of O−O band in phenol showing doublet structure.

TABLE I. The spectrum of phenol. The intensities are designated as *vw* = very weak, *w* = weak, *m* = median, *ms* = medium strong, *s* = strong, *vs* = very strong, and *vvs* = extremely strong, *B* = broad and *D* = diffuse. (Bands grouped together are the components of a doublet.)

Wavelength (Å)	Frequency (cm^{-1})	Intensity	Assignment
2827.93	35,351.2	*vvw*	0−999
19.09	35,462.0	*vvw*	0−824−61
18.76	35,466.2		
14.11	35,524.8	*w*	0−824
13.83	35,528.3		
13.04	35,538.3	*vvwB*	0−811
07.78	35,604.9	*vvw*	0−527−221
2800.55	35,696.8	*vvwB*	
2798.28	35,725.7	*vvwB*	0−999+374
95.62	35,759.5	*vvw*	0−527−61
95.34	35,763.3		
94.68	35,771.8	*vvw*	
94.43	35,774.9		
93.63	35,785.2	*vvwB*	
92.46	35,800.2	*vvwD*	
91.83	35,808.3	*vwB*	
91.15	35,817.0	*w*	
90.78	35,822.5	*m*	0−527 0−999+476
90.50	35,825.3		
85.27	35,892.6	*vw*	0−397−61
83.73	35,912.5	*vvw*	0−999+562 0−811+374
83.54	35,914.9		
80.71	35,951.5	*m*	0−397
79.00	35,973.6	*vvw*	
76.08	36,011.4	*vw*	0−811+476
75.89	36,013.6		
75.23	36,022.4	*vw*	
74.76	36,028.5	*vvw*	0−527+208
73.92	36,039.4	*vw*	
73.71	36,042.2		
72.66	36,055.8	*vvw*	
71.74	36,067.8	*vvw*	0−221−61
71.53	36,070.5		
70.19	36,088.0	*vvw*	0−824+562
69.99	36,090.6		
68.95	36,105.4	*vw*	0−245
68.74	36,106.9		
67.14	36,127.7	*s*	0−221
66.94	36,130.6		
2766.64	36,134.3	*vvwBD*	0−999+783
65.89	36,144.0	*vvw*	0−245+40
65.62	36,147.6		
65.37	36,150.9		
65.05	36,155.0	*vw*	
64.86	36,157.5		
64.63	36,160.5		0−397+208
63.27	36,178.2	*vw*	
63.08	36,180.8		
62.61	36,187.0	*vw*	
62.42	36,189.5		
62.11	36,193.5	*w*	0−527+374
61.89	36,196.4		
61.28	36,204.4	*w*	
61.09	36,206.9		
60.34	36,216.7	*vvw*	
60.10	36,219.9	*vvw*	
59.78	36,224.1	*w*	0−2×61
59.57	36,226.8		
58.63	36,239.2	*vwB*	
58.18	36,245.1	*vvw*	
57.96	36,248.0	*vvwB*	
57.59	36,252.9	*ms*	
57.38	36,255.6		
55.50	36,280.4	*vw*	
55.27	36,283.4		
54.95	36,287.6	*vvs*	0−61 (0−999+935)
54.74	36,290.7		
54.12	36,298.5	*m*	0−527+476
53.91	36,301.3		
53.18	36,310.9	*s*	0−824+783 0−245+208
52.96	36,313.8		
50.82	36,342.1	*vs*	
50.62	36,344.7		
50.29	36,348.6	*vvs*	0−0
50.08	36,351.9		
49.30	36,362.2	*vw*	
49.12	36,365.1		
47.72	36,383.1	*vvw*	
47.54	36,385.5	*vvw*	0−527+562
47.27	36,389.0	*s*	0+40
47.06	36,391.8		

TABLE I.—*Continued*

Wavelength (A)	Frequency (cm^{-1})	Intensity	Assignment
2746.59	36,398.0	*m*	
46.39	36,400.7		
45.39	36,415.1	*vvw*	
44.48	36,426.0	*vvwD*	0−397+476
43.38	36,440.6	*vvw*	
41.77	36,462.0	*vvwB*	0−824+935
41.04	36,471.7	*vvw*	
39.27	36,495.3	*vwBD*	0−61+208
38.68	36,503.2	*vw*	0−824+975 0−221+374
38.47	36,506.0		
36.99	36,525.7	*vvw*	
36.77	36,528.6		
36.05	36,538.3	*vvw*	
35.84	36,541.0		
35.08	36,551.2	*vvw*	
34.66	36,556.8	*ms*	0+208
34.47	36,559.4		
32.73	36,582.6	*vvwB*	0−245+476
31.50	36,599.1	*vvwB*	0+208+40
31.01	36,605.7	*wD*	0−221+476 0−527+783
30.79	36,608.8		
29.58	36,624.9	*vvwB*	0−999+1274
29.10	36,631.2	*vvwB*	
26.73	36,663 1	*vw*	0−245+562 0−61+374
26.52	36,666.0		
25.89	36,674.4	*w*	
25.71	36,676.9		
23.66	36,704.5	*vvw*	
22.92	36,714.3	*vvw*	
22.63	36,718.3		
22.31	36,722.7	*m*	0+374
22.09	36,725.6		
20.52	36,746.7	*vvw*	
19.73	36,757.5	*vvwB*	0−527−935
19.25	36,764.0	*vvw*	0−61+476
19.07	36,766.4		0+374+40 0+2×208
18.42	36,775.2	*vvw*	
17.51	36,787.5	*vvw*	
17.09	36,793.2	*vvw*	0−527+975
2716.19	36,805.4	*vvwB*	0+2×208+40
15.53	36,814.3	*wD*	0−811+1274
15.23	36,818.4	*wD*	
14.75	36,824.9	*vs*	0+476
14.58	36,827.2		
12.72	36,852.5	*vvwB*	0−61+562
11.85	36,864.3	*vvw*	0+476+40
11.68	36,866.6		
11.26	36,872.3	*vw*	
11.08	36,874.7		
10.12	36,887.8	*vw*	0−245+783 0−397+935
09.94	36,890.3		
08.39	36,911.4	*m*	0+562 0−221+783
08.20	36,914.0		
07.14	36,928.4	*vvw*	0−347+975 0+208+374
06.00	36,944.0	*vvw*	
04.80	36,960.4	*vvwB*	
04.09	36,969.8	*vvwB*	0+3×208
03.50	36,978.1	*vwB*	
02.87	36,985.9	*vw*	
02.72	36,988.8		
01.42	37,006.6	*vw*	
01.22	37,009.4		
2699.34	37,035.1	*w*	0−245+935 0+208+476 0−61+2×374
99.10	37,038.4		
98.03	37,053.1	*vvw*	
97.06	37,066.4	*wD*	0−221+935
96.75	37,070.7	*s*	0−61+783
96.58	37,073.0		
96.03	37,080.6	*m*	0−245+975
95.53	37,087.5	*vvwB*	0−824+1565
94.99	37,094.9	*m*	0+2×374 0−527+1274
94.77	37,097.9		
93.28	37,118.5	*wD*	0+208+562 0−811+1565
92.75	37,125.7	*msD*	
92.59	37,128.0		
92.27	37,131.5	*vvs*	0+783 0+2×374+40
92.10	37,134.7		
89.50	37,170.6	*m*	0+783+40
89.29	37,173.5		

TABLE I.—*Continued*

Wavelength (Å)	Frequency (cm^{-1})	Intensity	Assignment
2688.62	37,182.8	*vwD*	
87.89	37,192.9	*w*	
87.67	37,195.9		0+374+476
86.20	37,216.3	*m*	0+783+2×40
86.03	37,218.6		
85.75	37,222.5	*ms*	0−61+935 0−397+1274
85.50	37,226.0		
84.86	36,234.8	*w*	
84.62	37,238.2		
83.92	37,247.9	*w*	
83.67	37,251.3		
82.80	37,263.4	*mBD*	0−61+975
82.22	37,271.5	*mBD*	
81.91	37,275.8	*wD*	0−61+208+783
81.30	37,284.3	*vvs*	0+935 0+374+562
81.11	37,286.9		
80.90	37,289.8		
80.51	37,295.3	*ms*	
80.30	37,298.2		
79.65	37,307.2	*m*	0+2×374+208
79.48	37,309.6		
79.16	37,314.1	*wBD*	
78.47	37,323.7	*s*	0+975 0+935+40
78.22	37,327.2		0+2×208+562
			0−61+476+542
77.42	37,338.3	*w*	0+208+783
77.27	37,340.4		
76.79	37,347.1	*vvw*	
76.15	37,356.0	*vvw*	
75.51	37,365.0	*vvw*	0+975+40
74.63	37,377.3	*vvwB*	0−245+1274
73.77	37,389.3	*vwB*	0−527+1565
			0+476+562
73.39	37,394.6	*vvw*	
72.81	37,402.7	*vwB*	0−221+1274
70.62	37,433.4	*vwB*	0−61+208+935
69.59	37,447.8	*vvw*	0−61+374+783
68.94	37,456.9	*vvw*	
68.78	37,459.2		
68.25	37,466.6	*vvwD*	
2667.65	37,475.0	*vvw*	0+2×562
66.18	37,495.7	*vwB*	0+208+374+562
			0+208+935
65.36	37,507.2	*vvw*	0+374+783
65.18	37,509.7		0+208+2×476
64.54	37,518.8	*vvw*	0−397+1565
63.90	37,527.8	*vvwB*	0+208+975
62.83	37,542.9	*vvw*	0−61+476+783
61.57	37,560.7	*vw*	0−61+1274
61.37	37,563.5		
60.60	37,574.3	*vwB*	0+2×374+476
			0−527+476+1274
59.83	37,585.2	*vwD*	
59.17	37,594.5	*vvw*	0−61+374+935
			0+208+476+562
57.87	37,613.0	*w*	0+476+783
57.65	37,616.0		
57.18	37,622.7	*s*	0+1274
57.01	37,625.1		
56.24	37,636.0	*vvw*	0−61+562+783
			0−61+374+975
54.51	37,660.5	*vw*	0+1274+40 0+374+935
54.37	37,662.5		0+2×374+562
52.06	37,695.3	*vvwBD*	0−221+1565
			0+562+783 0+374+975
47.42	37,761.4	*ms*	0+476+935
47.26	37,763.7		0+374+476+562
46.90	37,768.8	*vvw*	0−61+208+1274
45.95	37,782.4	*vvw*	0−61+562+935
45.54	37,788.2	*vvw*	
44.80	37,798.8	*vvw*	0+476+975
44.01	37,810.1	*vvw*	
43.31	37,820.1	*vvw*	0+208+476+783
42.71	37,828.7	*vvw*	0+208+1274
41.64	37,844.0	*vvw*	0+562+935
			0+374+2×562
41.17	37,850.7	*w*	0−61+1565
40.97	37,853.6		

TABLE I.—*Continued*

Wavelength (Å)	Frequency (cm^{-1})	Intensity	Assignment
2640.50	37,860.3	*vvw*	0+2×476+362
39.31	37,877.4	*vwBD*	
38.87	37,883.7	*vvw*	0+562+975 0+2×374+783
38.40	37,890.5	*vvw*	
37.83	37,898.5	*vvwB*	0+208+562+783
36.74 36.64	37,914.3 37,915.8	*s*	0+1565 0+2×783
36.12	37,923.3	*vvw*	
34.50	37,946.6	*vvwBD*	0+476+2×562
33.44	37,961.6	*vvw*	
32.73	37,972.1	*vvw*	0+208+476+935
30.99	37,997.2	*vvw*	0+374+1274
30.48	38,004.6	*vBD*	0+208+476+965
29.70	38,015.8	*vvw*	
28.65	38,031.0	*vvw*	0+2×374+935
27.85	38,042.6	*vvw*	0−61+783+935
26.71	38,059.1	*wD*	0−61+208+1565
26.32	38,064.7	*msD*	
26.12 25.86	38,067.7 38,071.4	*vs*	0+783+935
25.49 25.33	38,076.8 38,079.3	*w*	
24.65	38,089.0	*vw*	
24.24	38,094.9	*vw*	0+208+562+975
23.80	38,101.3	*vvw*	0+476+1274
23.51 23.37	38,105.5 38,107.4	*m*	0+783+975
22.55	38,119.6	*vvwB*	0+208+1565 0+208+2×783
21.68	38,132.1	*vvwB*	0+374+476+935
20.75	38,145.7	*vvw*	
19.99	38,156.7	*vvwB*	0−61+2×935
19.10	38,169.7	*vvwB*	0+476+562+783
18.16	38,183.4	*vvw*	0+562+1274
17.17	38,197.8	*vvw*	0−61+935+975
16.08	38,213.7	*vvwB*	
2615.71 15.55	38,219.1 38,221.5	*msD*	0+2×935
14.80	38,232.4	*vwB*	0+2×476+935
13.84	38,246.5	*vwBD*	
12.90	38,260.2	*vwD*	0+2×935+40 0+935+975
11.76	38,277.0	*vvwB*	0+2×476+975 0+208+783+935
10.70	38,292.5	*vvwB*	0+374+2×783
09.66	38,307.7	*vvwB*	0+208+476+1274
08.42	38,326.0	*vvwB*	0+476+562+935
07.20	38,343.9	*vvw*	0+61+783+1274
05.58	38,367.7	*vvw*	0+2×374+1274
03.57	38,397.3	*wBD*	0+208+562+1274
02.98	38,406.0	*msB*	0+783+1274 0+2×562+935
00.40	38,444.1	*vvw*	0+374+783+935 0+2×562+975
2596.84	38,497.0	*vvw*	0−61+935+1274 0+208+374+1565
93.57 93.21	38,545.4 38,550.7	*vw*	0+476+783+935
92.76 92.54	38,557.4 38,560.7	*m*	0+935+1274
92.04	38,568.1	*vvw*	
90.39 90.18	38,592.7 38,595.8	*vw*	0+374+2×935 0+975+1274
88.12	38,626.5	*vvw*	0+562+783+935
87.66	38,633.4	*vvw*	0+374+935+975
83.55	38,695.9	*vBD*	0+3×783 0+476+2×935
81.24	38,729.5	*vvwD*	
78.38	38,772.4	*vvwD*	0+476+2×975
77.36	38,787.8	*vvwBD*	
73.29	38,849.1	*wBD*	0+935+1565
72.74	38,857.4	*vvw*	
72.20	38,865.6	*vvw*	0+2×476+1565
71.58	38,875.0	*vvw*	

TABLE I.—*Continued*

Wavelength (A)	Frequency (cm^{-1})	Intensity	Assignment
70.81	38,886.6	*vwB*	0+975+1565
70.28	38,894.7	*vw*	0+2×1274
69.30	38,909.5	*vvw*	
67.50	38,936.7	*vvwBD*	
63.30	39,000.5	*vw*	0+783+2×935
63.17	39,002.5		0+208+2×1274
61.63	39,026.0	*vvwB*	0+476+935+1274
60.71	39,040.0	*vvwD*	0+2×562+1565
			0+783+935+975
53.41	39,151.6	*vvwD*	0+3×935
51.10	39,187.0	*vvwBD*	0+1274+1565
41.88	39,329.2	*vvw*	
41.27	39,338.6	*vvw*	0+783+935+1274
41.04	39,342.2		
2539.54	39,365.4	*vvw*	0+476+975+1565
38.85	39,376.1	*vvwB*	0+476+2×1274
			0+783+975+1274
34.44	39,444.6	*vvw*	
32.10	39,481.0	*vvwD*	0+4×783 0+2×1565
29.01	38,529.3	*vvwD*	0+935+975+1274
22.67	39,628.6	*vvwBD*	0+762+935+1565
20.14	39,668.4	*vvwBD*	0+783+975+1565
13.02	39,780.8	*vvwBD*	0+2×935+1565
10.42	39,822.0	*vvwBD*	0+935+975+1565
03.30	39,935.2	*vvw*	
01.01	40,080.7	*vvw*	
2491.65	40,122.0	*vvw*	0+935+1274+1565

TABLE II. Fundamental vibrational frequencies of phenol.

Ground state						Excited state		
Ultraviolet			Raman					
Masaki	Asagoe, Shimokawa, Kageyama	This research	Masaki	Kahovec, Reitz	Kohlrausch, Wittek	This research	Hall	Asagoe, Shimokawa, Kageyama
228	(235)	245 *w*	235	242 (6*b*)	240 (5)	208 *ms*		
		397 *m*				374 *m*		
528	(526)	527 *m*	526	532 (5)	532 (5)	476 *vvs*	478	473
604	(614)	623 *vvw*	614	617 (5)	617 (8)	562 *m*		
820		811 *wwb*	813	812 (8*b*)	812 (10*b*)	783 *vvs*	782	779
		824 *w*		826 (3)	829 (12*b*)			
	Reported as differences	999 *ww*		1000 (2)	1001 (10)	935 *vvs*	935	932
				1025 (8)	1026 (7)	975 *vvs*		982
				1253 (4*b*)	1250 (2*b*)	1273 *s*		1273
				1598 (5*d*)	1595 (6)	1565 *s*		

DISCUSSION

The 0−0 transition, the most intense band in the spectrum, appeared as a doublet (see Fig. 2), the wave numbers of the components being 36,348.6 and 36,351.9 to be compared with the frequencies given for a single band of 36,351 cm^{-1} reported by Hall and 36,356 reported by both Masaki, and by Asagoe, Shimokawa, and Kageyama.

The $0-1\times\nu_i$ [9] transitions 245, 526, 811, and 999 cm^{-1} were found corresponding to the symmetrical Raman frequencies 242, 532, 812, and 1000 cm^{-1} reported by Kahovec and Reitz (Table II). In addition, a band of medium intensity was found 824 cm^{-1} to the red of the 0−0 band which probably corresponds to the antisymmetric Raman frequency 826 cm^{-1}. If this association is correct, it is the first instance in our work of an antisymmetric vibration entering into the spectrum in this way. The 617 cm^{-1} Raman frequency did not appear as $0-1\times\nu_i$ transition although Masaki reported a band 604 cm^{-1} to the red from 0−0, and Asagoe, Shimo-

[9] ν will be used to represent fundamental frequencies in the ground state, and ν' in the excited state.

kawa, and Kageyama reported 614 as an important difference frequency.

The medium band 397 cm^{-1} to the red from $0-0$ has also been taken as $0-1\times\nu$ even though it is missing in the Raman spectrum. Other monosubstituted benzenes have a strong Raman line in this neighborhood, and in fact, Kahovec and Reitz leave a space for this frequency in their table. In addition, this frequency combined well with a number of frequencies in the excited state. It was thought to be the same mode of vibration as the strong frequency 374 of the excited state.

The low intensity of 623, 811, and 999 cm^{-1} even at high phenol pressures and high cell temperatures seemed to indicate some selection rule against their appearance. All three have a greater Raman intensity (8, 10, and 10, respectively) than 532 (intensity 5) which appeared strongly even at low phenol pressures and low cell temperatures. That the Boltzmann factor does not account for this low intensity may be seen from the ratios of the Boltzmann factors of the three higher frequencies to the Boltzmann factor of the 532 frequency; these are 0.67, 0.26, and 0.11, respectively, at a temperature of 27°C.

In addition to the frequencies which may be correlated with the Raman data there appeared two strong bands 61 and 221 cm^{-1} to the red from the $0-0$ band. These may be difference frequencies and because of the high intensity probably involve a low frequency in the ground state. These combined with a number of frequencies in the excited state. Hall reported values of 60 and 218 cm^{-1} while Asagoe, Shimokawa, and Kageyama reported 60 and 220 cm^{-1}.

The identification of fundamental frequencies in the excited state was difficult because only an indirect correlation with the Raman data was possible and because of the large number of bands in the phenol spectrum. The bands were so closely spaced that if frequencies were chosen at random, the probability of coincidence (3 cm^{-1}) was between 0.4 and 0.5.

The fundamental frequencies in the excited state were chosen on the following basis: the intensity of the $0+1\times\nu_i'$ transition, the correlation with Raman and ground-state frequencies, and the combinability with other chosen frequencies. These frequencies are listed in Table II opposite the Raman frequencies with which they are probably associated. The association was made with all the strong totally symmetric frequencies with the exception of 1274. Asagoe, Shimokawa, and Kageyama have associated the 1272 excited state frequency (1274 in this research) with the Raman line, 1252. This is not an impossible association, but it is generally believed that electronic excitation loosens the molecule so that the vibration frequencies of the excited state would be smaller than those of the ground state.

A strong band appeared 40 cm^{-1} to the blue from the 0^1-0 band. This combined strongly with all the fundamental frequencies in the excited state and with many combinations of these fundamental frequencies. It did not, however, combine with any of the frequencies in the ground state.

Due to the fact that the assignment of fundamental frequencies (either the choice of the frequency or its precise value to a single wave number) was not absolutely certain, that all possible combinations of the fundamental frequencies did not appear, and that a high probability for accidental coincidences existed, the situation with regard to the combination bands was unsatisfactory. In this research a large number of observed frequencies were left unassigned because the authors could not be certain from the data that transitions of the type $0-1\times\nu_i+1\times\nu_j'+1\times\nu_k'$ were present. Some assignments of the type $0+1\times\nu_i'+1\times\nu_j'+1\times\nu_k'$ were included even though a number of this type were missing.

All two-quantum number transitions, $0+2\times\nu_i'$ and $0+1\times\nu_i'+1\times\nu_j'$ were present with the exception of $0+526+40$. A large number of the three-quantum number transitions were missing. Among the better series were $0+783+935+1\times\nu_k'$ of which no members were missing, and $0+2\times935+1\times\nu_j'$ which did not contain 208, 476, and 562.

It would seem that further work on the monosubstituted benzenes should take away some of the uncertainty in making the assignments and lead to the formulation of definite selection rules if they exist. Research of such character is in progress in this laboratory.

The authors acknowledge with gratitude, the continued support of the University of Texas Research Institute.

The Structure of Liquid Argon

LOUIS H. LUND
*University of Missouri, Columbia, Missouri**

The method of Wall for calculating the free volume per atom in a liquid has been applied to liquid argon, using the atomic distribution curves at 84.3°K and at 91.8°K given by Eisenstein and Gingrich. From the free volumes at these temperatures, the entropy of the liquid at the boiling point is calculated to be 15.8 cal. degree^{-1} mole^{-1}. This value, together with the calculated entropy, 32.2 cal. degree^{-1} mole^{-1}, of argon vapor at the boiling point, give an entropy of vaporization of 16.4 cal. degree^{-1} mole^{-1}. The latent heat of vaporization is thus calculated to be 6.01 kilojoules per mole; this is to be compared with the observed value of 6.3 kilojoules per mole. Presented also is a comparison of theoretical and experimental atomic distribution curves at the temperatures, 84.3°K and 91.8°K.

1. INTRODUCTION

ONE of the most fundamental characteristics of a liquid is its structure. Compared to the structure of a crystal, the structure of a liquid is much less evident, much less exact over extended regions, and in a microscopic sense much less simply specified. Perhaps the best description of the structure of a liquid that can be given is a "statistical" one in terms of its atomic, or molecular, distribution curve[1] which gives the average number of atoms between distances R and $R+dR$ from any arbitrarily chosen atom in the body of the liquid. The ultimate utility of these curves arises from the fact that they present a graphical representation of time-averaged atomic or molecular arrangements induced under the action of characteristic interatomic or intermolecular forces.

Several different approaches have been attempted to determine these distribution curves, and some attempts have been made to use them in deducing macroscopic properties of elementary substances. They have been determined[2] directly from experimental data, and they have been obtained[3] from several theoretical approaches which rely in different ways on experimental data for the evaluation of otherwise unknown parameters. Thus far, the diffraction of x-rays by liquid elements has supplied[2] the majority of known distribution curves for relatively simple liquids, and some of these[4] have been used in simplified calculations to obtain quantities such as heats of fusion or vaporization.

The liquids sodium, potassium, and argon have been the subjects of special studies. Kirkwood and Boggs[5] applied a general method to obtain an approximate solution for the radial distribution function of a system of "hard spheres;" they then compared this to experimentally obtained distribution curves for argon. Rushbrooke[6] calculated the shape of the first peak on the distribution curve for liquid argon on the basis of the Lennard-Jones and Devonshire theory[7] of the liquid state of inert gases. In the present work, Wall's theory[8] has been applied to curves obtained by Eisenstein and Gingrich[9] for liquid argon at $T=84.3$°K and $T=91.8$°K.

2. THEORY

Wall's theory[8] assumes a simple model of the quasi-solid type in which each atom is trapped by its immediate neighbors in a small spherical cell. The potential energy function within the cell is assumed to be a discontinuous "box" type

* Now with the Laboratory, Lukas-Harold Corporation, operators of the U. S. Naval Ordnance Plant, Indianapolis, Indiana.

[1] P. Debye and H. Menke, Physik. Zeits. **31**, 379 (1930).

[2] N. S. Gingrich, Rev. Mod. Phys. **15**, 90 (1943).

[3] J. G. Kirkwood and E. M. Boggs, J. Chem. Phys. **10**, 394 (1942); J. Corner and J. E. Lennard-Jones, Proc. Roy. Soc. **A178**, 401 (1941); G. S. Rushbrooke and C. A. Coulson, Phys. Rev. **56**, 1216 (1939); C. N. Wall, Phys. Rev. **54**, 1062 (1938); J. A. Prins and Petersen, Physica **3**, 147 (1936).

[4] C. N. Wall, Phys. Rev. **54**, 1062 (1938); N. S. Gingrich and C. N. Wall, Phys. Rev. **56**, 336 (1939); J. H. Hildebrand, J. Chem. Phys. **7**, 1 (1939).

[5] J. G. Kirkwood and E. M. Boggs, J. Chem. Phys. **10**, 394 (1942).

[6] G. S. Rushbrooke, Proc. Roy. Soc. Edinburgh **60**, 182 (1940).

[7] J. E. Lennard-Jones and A. F. Devonshire, Proc. Roy. Soc. **A163**, 53 (1937).

[8] C. N. Wall, Phys. Rev. **54**, 1062 (1938).

[9] A. S. Eisenstein and N. S. Gingrich, Phys. Rev. **62**, 261 (1942).

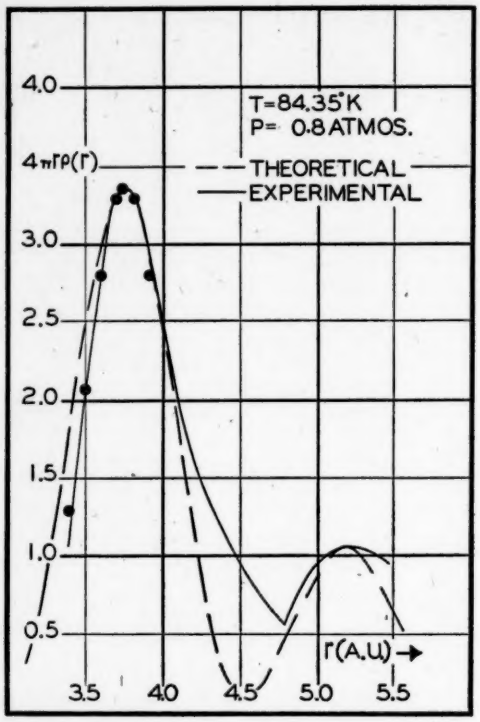

FIG. 1. A comparison of theoretical and experimental atomic distribution curves for $4\pi R\rho(R)$ *vs.* R for liqud argon at 84.3°K. Solid line is experimental. Dotted line is theoretical (σ by R−C method). Circles are theoretical values (σ by iteration).

in which the potential is practically constant throughout the cell except at the cell boundary where it becomes infinite. This implies a uniform probability of finding the atom within equal volumes of the cell. The analytical expression he derives for the distribution function is

$$4\pi R^2\rho_1(R)=\frac{3N_1R}{5\sigma R_1}\left\{1-\frac{5(R_1-R)^2}{4\sigma^2}\times\left[1-\frac{|R_1-R|}{2\sigma}+\frac{|R_1-R|^3}{40\sigma^3}\right]\right\} \quad (1)$$

for

$$R_1-2\sigma\leqq R\leqq R_1+2\sigma,$$

and

$$4\pi R^2\rho_1(R)=0$$

for all other values of R.

In this expression, $\rho_1(R)$ is the density of nearest neighbors surrounding an atom in the liquid, i.e., the density of those atoms whose cell centers lie on the first co-ordination sphere of radius R_1, $4\pi R^2\rho_1(R)dR$ is the number of nearest neighbors between distances R and $R+dR$ from a given atom, N_1 is the average number of nearest neighbors of a given atom, σ is the radius of the sphere whose volume represents the free volume for the trapped atom (i.e., its center) within it. It is assumed that the density of nearest neighbors, $\rho_1(R)$, is practically the total density of atoms in the interval $0\leqq R\leqq R_1$ and hence that in this interval, Eq. (1) is the atomic distribution function for the liquid.

If it is desired to extend the range of the distribution curve, it is necessary to consider density contributions from atoms whose cell centers lie on co-ordination spheres of order higher than the first. If ρ_i is the density contribution of the N_i atoms lying on the co-ordination sphere of radius R_i, then the total distribution curve is given by

$$4\pi R^2\rho(R)=4\pi R^2\sum_{i=1}\rho_i(R), \quad (2)$$

where $\rho_i(R)$ is given by an equation of the same form as (1) with N_1 and R_1 replaced by N_i and R_i. For the present, we shall restrict the calculations to the interval $0\leqq R\leqq R_1$.

3. APPLICATION TO LIQUID ARGON

The parameters σ, N_1, R_1 are found by fitting the distribution function (1) to the experimental values for liquid argon. Using for convenience, $4\pi R\rho_1(R)$ rather than $4\pi R^2\rho_1(R)$, Eq. (1) may be written in the form

$$\sigma^2=\frac{y_1}{y_1-y}\times\frac{5(R_1-R)^2}{4}\times\left[1-\frac{|R_1-R|}{2\sigma}+\frac{|R_1-R|^3}{40\sigma^3}\right], \quad (3)$$

where $y=4\pi R\rho_1(R)$ and $y_1=3N_1/5\sigma R_1$ and is the

TABLE I. Calculated values of σ by iteration.

$T=84.3$°K			$T=91.8$°K		
R (A)	$4\pi R\rho_1(R)$ (exp)	σ (A) (calc)	R (A)	$4\pi R\rho_1(R)$ (exp)	σ (A) (calc)
3.4	1.07	0.34	3.2	0.37	0.43
3.5	2.09	0.37	3.3	0.82	0.44
3.6	2.77	0.36	3.4	1.31	0.44
3.7	3.31	0.42			
Average		0.37A	Average		0.44A
$R_1=3.75$A			$R_1=3.74$A		
$y_1=3.36$			$y_1=2.48$		
$N_1=7.8$ atoms			$N_1=6.8$ atoms		

maximum value of y. From the experimental values of $4\pi R^2\rho_1(R)$, a table of y *vs.* R may be constructed and y_1 and R_1 are thus immediately found. σ may then be found by solving (3) by iteration for several paired experimental values of R and y. Table I shows the experimental values of $4\pi R\rho_1(R)$ and the calculated values of σ for several values of $R<R_1$ for liquid argon at 84.3°K and 91.8°K. Clearly the agreement between the values of σ calculated in this manner at each temperature is quite good.

Rushbrooke and Coulson[10] (hereafter referred to as R−C) have proposed two somewhat simplifying relations to determine the parameters σ and N_i. They are

$$N_1/N_i=R_1y_1/R_iy_i, \tag{4}$$

$$1+N_1+(N_2/2)=(4/3)\pi R_1^3\rho_0, \tag{5}$$

where y_i is the value of $4\pi R\rho(R)$, corresponding to R_i, and ρ_0 is the average macroscopic density of the liquid in atoms per unit volume. Equation (4) follows directly from (1), and (3) from the assumption that if we take a small imaginary sphere of radius R_1 situated anywhere at random in the liquid it will enclose the same number of atoms, no matter where it might be in the liquid. σ may then be found by noting that if in Eq. (1) $R=R_1$, then

$$y_1=3N_1/5R_1\sigma. \tag{6}$$

It is interesting to note that values of σ calculated by this last method are 0.37A for $T=91.8$°K and 0.45A for $T=84.3$°K (see Table II). These are just the reverse of the values obtained by the iteration method above. Since the R−C proposal depends on the rather precise location of R_1 and y_1 from the experimental curve, while, on the other hand, by an iteration process such as has been used, one uses an extended portion of the experimental curve, it would seem preferable to use the latter method. Furthermore, in the cases of liquid sodium and potassium,[4] σ increased with increasing temperature which is more reasonable than the results obtained by this particular application of the R−C method to liquid argon.

TABLE II. Calculated N's and σ's (R−C).

$T=91.8$°K	$T=84.3$°K
$R_1=3.74$A $R_2=4.6$A	$R_1=3.75$A $R_2=5.2$A
$y_1=2.48$ $y_2=1.26$	$y_1=3.36$ $y_2=1.04$
$N_1=5.66$ atoms	$N_1=9.48$ atoms
$N_2=3.54$ atoms	$N_2=4.07$ atoms
$\sigma=0.37$A	$\sigma=0.45$A
$\rho_0=0.0207$ atoms/A^3	$\rho_0=0.0212$ atoms/A^3

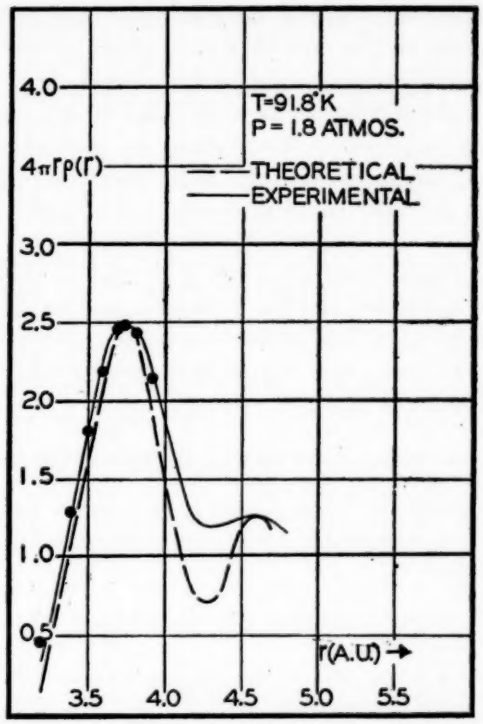

FIG. 2. A comparison of theoretical and experimental atomic distribution curves for $4\pi R\rho(R)$ *vs.* R for liquid argon at 91.8°K. Solid line is experimental. Dotted line is theoretical (σ by R−C method). Circles are theoretical values (σ by iteration).

Figures 1 and 2 show theoretical distribution functions using the sigmas obtained by both methods. Each R−C distribution curve (dotted) represents an extended distribution curve and hence as indicated in Eq. (2) is a summation, in the interval where this is possible, of two theoretical distribution equations of the form given by Eq. (1); Table II shows the N's and values of σ for each curve. These extended R−C curves agree reasonably well with the experimental curves in their general aspects, but in both cases the saddle between the experimental peaks does not fall to as low a value as does that for the theoretical curve. This low value to which

[10] G. S. Rushbrooke and C. A. Coulson, Phys. Rev. **56**, 1216 (1939).

the theoretical curve falls in each case is due primarily to the fact that the interval in which the two theoretical distribution equations add is a very small interval, $4\sigma-(R_2-R_1)$. This interval in the one case is 0.42A, and in the other is 0.35A; furthermore, the two functions themselves are quite small in the interval where they add.

The theoretical points represented by circles (σ by iteration) in Figs. 1 and 2 agree very well indeed with the experimental curves and would seem to verify the values of σ obtained in this manner.

4. THERMODYNAMIC APPLICATION

Guggenheim[11] has shown that the free energy of a simple liquid is given approximately by the equation

$$F=-NkT[\ln J(T)+\ln v]+\varphi, \qquad (7)$$

where φ is the minimum potential energy of the molecular assembly and $J(T)$ is the ordinary partition function of the molecule. For a monatomic liquid at moderate temperatures, $J(T)$ may be supposed to take its classical value $[2\pi mkT/h^2]^{\frac{3}{2}}$ and v is the free volume per atom. The other symbols have their usual significance.

Differentiating Eq. (7), we obtain for the entropy of liquid argon

$$S_L=-\left(\frac{dF}{dT}\right)_V=Nk\left[\ln J(T)+\ln\frac{4}{3}\pi\sigma^3+\frac{3}{2}+\frac{3}{\sigma}T\frac{d\sigma}{dT}\right]. \qquad (8)$$

[11] E. A. Guggenheim, Proc. Roy. Soc. **A135**, 181 (1932).

Using the values $\sigma_{84.3}=0.37$A and $\sigma_{91.8}=0.44$A, by ordinary linear interpolation we have $\sigma_{87.3}=0.40$A for the value of σ at the boiling point of liquid argon, and $0.07/7.5=d\sigma/dT|_{T=87.3}$ for an approximate value of $d\sigma/dT|_{T=87.3}$. This rough interpolation and averaging process is all that can be reasonably attempted since the temperature range represented by the known values of σ is quite small. The value of the entropy of liquid argon at the boiling point calculated by this last equation with conversion from ergs to calories is 15.8 cal. degree^{-1} mole^{-1}.

The approximate entropy of the vapor may be calculated from the equation[12]

$$S_V=Nk\left\{\ln\left[\frac{2\pi mkT}{h^2}\right]^{\frac{3}{2}}+\ln\frac{V}{N}+\frac{5}{2}+\ln 2\right\}, \qquad (9)$$

where V is the volume per mole at the boiling point. This calculation gives $S_V=32.2$ cal. degree^{-1} mole^{-1}. The entropy of vaporization is thus 16.4 cal. degree^{-1} mole^{-1}. Since the heat of vaporization is

$$H=T_{\text{b.p.}}(S_V-S_L), \qquad (10)$$

the corresponding heat of vaporization for argon at its b.p. is 6.01 kilojoules per mole. The observed value is 6.3 kilojoules per mole.[13] The fairly close agreement between the observed and calculated values for this heat of vaporization is good, considering the approximations used and the neglect of communal entropy in the calculations.

[12] R. H. Fowler, *Statistical Mechanics* (Cambridge University Press, New York, 1936), second edition, p. 192, Theorem 6.31.

[13] *International Critical Tables*, Vol. 1.

Deviations from Stoichiometric Proportions in Cuprous Iodide*

ROBERT J. MAURER**
Laboratory for Insulation Research, Massachusetts Institute of Technology, Cambridge, Massachusetts

(Received February 23, 1945)

The absorption of iodine by cuprous iodide has been studied by means of a quartz microbalance. At 132.1°C the concentration of absorbed iodine varies as the square root of the pressure of iodine vapor in equilibrium with the sample. The temperature dependence of the the reaction at constant iodine vapor pressure indicates a heat of reaction of 0.24 ev per atom absorbed. The electrical conductivity of cuprous iodide at 132.1°C varies approximately as the 4/3 power of the concentration of the absorbed iodine.

INTRODUCTION

A FUNDAMENTAL problem in the investigation of semi-conducting compounds is the dependence of the electrical conductivity upon the deviation from stoichiometric proportions. This deviation is ordinarily so small as to prohibit direct measurement by chemical or physical methods.

In 1909, Baedeker[1] discovered that cuprous iodide, at room temperature, will absorb as much as 10^{-3} gram of excess iodine per gram of cuprous iodide. The resulting electrical conductivity was electronic in nature but of the "defect" type, the Hall constant being anomalous in sign. Nagel and Wagner[2] have shown that, if cuprous iodide is in equilibrium with iodine vapor, at constant temperature, the conductivity is a complicated function of the iodine vapor pressure.

In the light of Baedeker's results it seemed feasible to determine the concentration of excess iodine in cuprous iodide, as a function of the equilibrium iodine pressure and of the temperature, by direct weighing with a microbalance. Since equilibrium between the cuprous iodide and iodine vapor is established in a time of the order of minutes, it is necessary to operate the microbalance in an atmosphere of iodine vapor.

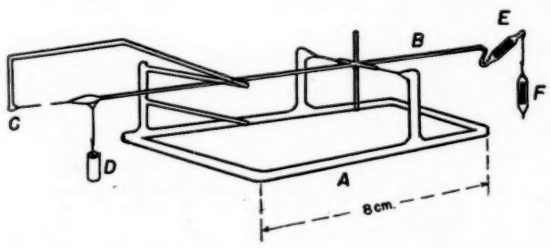

FIG. 1. Quartz microbalance.

EXPERIMENTAL PROCEDURE

The balance, illustrated in Fig. 1, is an adaptation of the type successfully used for the comparison of gas densities.[3,4] It was constructed of fused quartz, which was the only material exposed to the iodine vapor. The balance was operated as a null instrument, remote control being achieved in the manner described by Blewett.[5]

The frame, *A*, was of heavy fused quartz rod. The beam, *B*, was constructed of six pieces of half-millimeter quartz rod which were fused together, mutually at right angles, with the aid of a graphite jig. Two of the pieces formed the beam proper and the two short vertical rods were used to adjust the center of gravity. The remaining two quartz rods were cut off short and quartz fibers fused to them. These quartz fibers supported the beam, being fused to the heavy frame. The fibers were slightly slack so as to exert negligible restoring torque. The fiducial pointer, *C*, established the zero of the balance. The iron cylinder *E*, which was sealed in a thin-walled quartz capillary made an angle of about

* Publication No. 12 of the Solar Energy Conversion Research Program.

** Now at the Carnegie Institute of Technology, Pittsburgh, Pennsylvania.

[1] K. Baedeker, Ann. d. Physik **29**, 566 (1909).

[2] K. Nagel and C. Wagner, Zeits. f. physik. Chemie **B25**, 71 (1934).

[3] A. Stock and G. Ritter, Zeits. f. physik. Chemie **A119**, 333 (1926).

[4] M. Woodhead and R. Whytlaw-Gray, J. Chem. Soc. **209**, 846 (1933).

[5] J. Blewett, Rev. Sci. Inst. **10**, 231 (1939).

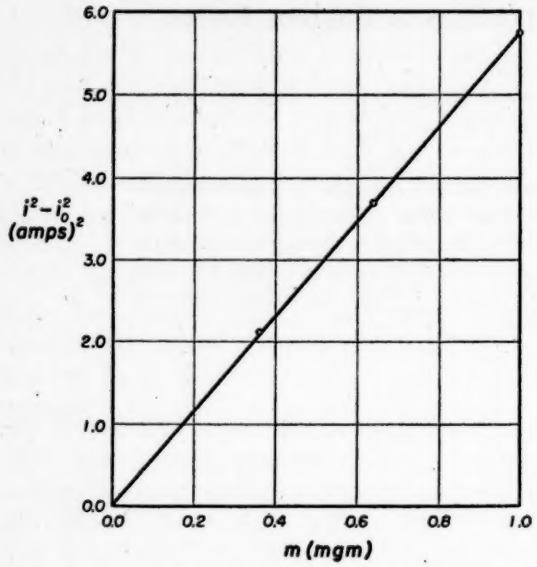

FIG. 2. Calibration curve of quartz microbalance.

20 degrees with the beam. This iron cylinder was 5.0 mm long and 1.0 mm in diameter.

The horizontal magnetic field of a pair of Helmholtz coils was used to create the torque upon the iron cylinder which deflected the beam. A set of storage batteries supplied the current for the coils.

An important detail in the construction of the balance was the method of suspending the specimen, D, and its counterweight, F, from the beam. They were hung on quartz fibers which were fused to the beam. Only in this manner was it possible to maintain the lever arm of the balance constant and avoid erratic apparent changes in weight of the specimen.

The counterweight, F, was a piece of platinum wire sealed in a quartz capillary. Its density was adjusted to within a few percent of the density of cuprous iodide so as to avoid buoyancy effects.

The balance was calibrated by placing known weights of aluminum wire on the specimen hook and determining the current necessary to bring the beam back to its zero. The aluminum wire was weighed upon an Ainsworth microbalance. The calibration was performed by first placing upon the specimen hook an unknown mass sufficient to bring the beam pointer slightly below the fiducial pointer. The current to balance the beam was i_0. The known mass, m, was then added to the specimen hook and the current for balance was i. Figure 2 shows a calibration curve. In agreement with the theory of the balance, $i^2-i_0^2$ was proportional to m. The zero of the balance was observed over a period of several weeks and remained constant within a fraction of a microgram.

The reliability and precision of the instrument were tested by mounting it in a Pyrex tube with a molybdenum weight on the specimen hook. At room temperature, the apparent change in weight of the molybdenum was determined as a function of the pressure of dry nitrogen in the tube. The data are shown in Fig. 3.

Figure 4 shows the experimental arrangement for determining the dependence of the weight of a cuprous-iodide specimen upon the equilibrium pressure of iodine vapor. The balance was in the Pyrex tube, T. The Helmholtz coils H, surrounded the Pyrex tube. The entire assembly was in the electrically heated oven, O. Two small, double-walled, mica windows permitted observation of the beam and fiducial pointer. A simple lens giving a magnification of 5-fold was used for this purpose. The Pyrex tube, E, which connected the balance tube with the iodine reservoir, A, was wrapped with a heating element and kept at a temperature intermediate of that of the balance and iodine.

Before assembly of the apparatus a sample of 0.5-mil copper foil was suspended from the specimen hook. The weight of foil chosen was such as to yield a weight of cuprous iodide approximately 10^{-5} gram in excess of that necessary to balance the counterweight. The capsule, D,

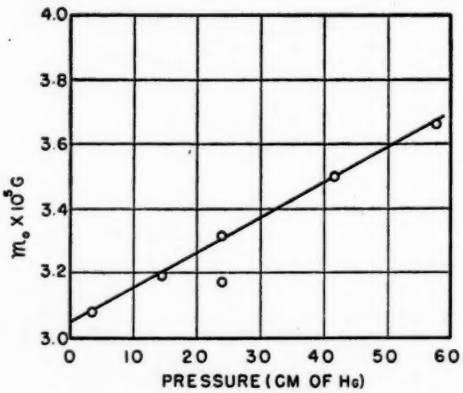

FIG. 3. Test of quartz microbalance

contained iodine which had been presublimed in a stream of dry nitrogen. After evacuating the tube through B, the capsule D was opened by dropping the glass-enclosed iron hammer S, on the thin-walled glass tip, C. The iodine was then distilled into the lower part of the tube E. Finally, after pumping the tube to a pressure of 10^{-6} mm Hg, it was sealed off at A.

The copper foil was slowly transformed to cuprous iodide by holding the balance oven at 150°C and the iodine oven at 80°C.

The oven temperatures were held constant by mercury thermoregulators and relays and the vapor pressure of the iodine in the tube was determined from the temperature of the iodine oven by use of the vapor pressure data of the *International Critical Tables*.

While taking data, the zero of the balance was checked periodically by immersing the iodine in liquid air and thus reducing the vapor pressure of iodine in the tube to a negligible value.

Figure 5 shows the dependence of the density of absorbed iodine atoms upon the pressure of the iodine vapor in equilibrium with the cuprous iodide. The temperature of the cuprous iodide was 132.1°C. The density of the absorbed iodine was calculated from the initial weight of the pure cuprous iodide and its measured change in weight. Since the initial weight of the copper foil was 29.414 milligrams, the initial weight of the cuprous iodide was taken as 88.14 milligrams. At all but the lowest iodine vapor pressures, the density of iodine atoms is proportional to the square root of the iodine vapor pressure.

$$d = d_0 p_{I_2}^{\frac{1}{2}}. \quad (1)$$

Figure 6 shows the dependence of the density of absorbed iodine atoms upon the temperature of the cuprous iodide for a constant equilibrium vapor pressure of iodine of 1.55 mm Hg. Over the narrow temperature interval examined, the density of absorbed iodine atoms is an exponential function of the reciprocal of the absolute temperature. The slope of the $\log_{10} d$ *versus* $1/T$ curve shown in Fig. 6 gives the heat of reaction as 0.24 electron volts per atom absorbed.

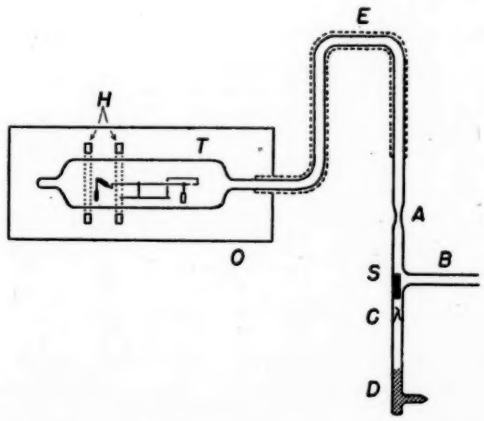

FIG. 4. Apparatus for investigation of absorption of iodine by cuprous iodide.

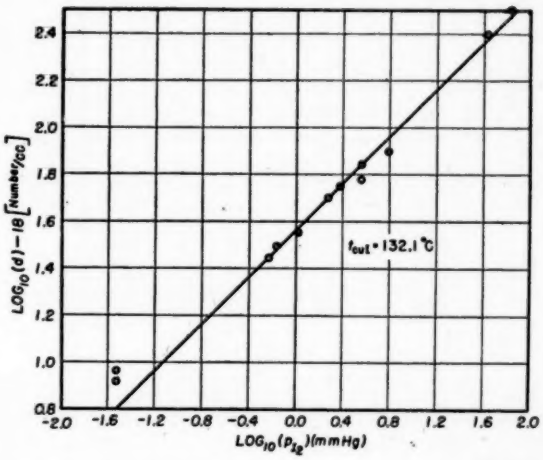

FIG. 5. The density of absorbed iodine atoms as a function of the equilibrium pressure of iodine vapor at constant temperature, $t = 132.1$ degrees C.

ELECTRICAL CONDUCTIVITY

The electrical conductivity of cuprous iodide was also measured as a function of temperature and of the equilibrium pressure of iodine vapor. Nagel and Wagner have shown that the increased conductivity, which results from the absorption of iodine, is electronic in nature. The electrolytic conductivity (due to the Cu^+) is also increased but is negligible. The experimental arrangement, which was essentially that of Nagel and Wagner,[2] is illustrated in Fig. 7. Platinum-foil electrodes were spot welded to two strips of copper foil, whose dimensions were 2.0 cm×0.5 cm×1.2×10^{-3} cm. The copper foils were suspended on platinum springs, spot welded to the electrodes, inside a sealed-off, evacuated Pyrex tube. Iodine, which had been

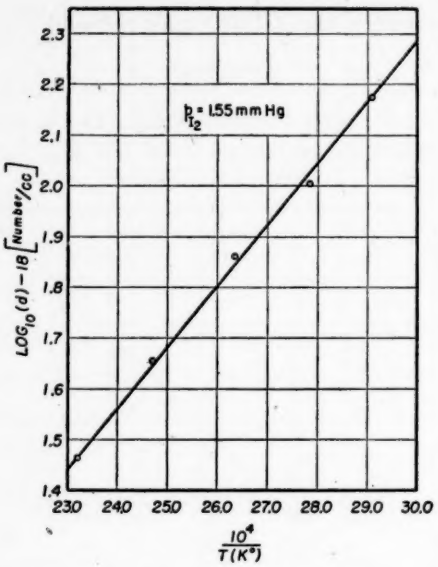

FIG. 6. The density of absorbed iodine atoms as a function of the temperature at constant iodine pressure. $pI_2 = 1.55$ mm Hg. Heat of reaction = 0.24 ev per atom absorbed.

presublimed in a stream of dry nitrogen, was distilled into the tube prior to its final evacuation and sealing off. That part of the tube containing the copper foils was surrounded by an electrically heated oven, O_1. The tube, E, which connected the specimen chamber, S, with the iodine reservoir, D, was wrapped with an electrical heating element and kept at a temperature intermediate of that of the ovens, O_1, and O_2. The oven temperatures were controlled by thermoregulators and measured with thermocouples and mercury thermometers. The resistance of the cuprous iodide was measured with a Leeds and Northrup Wheatstone bridge. The independence of the resistance of the cuprous iodide of the magnitude and sign of the d.c. voltage across the sample was checked. The resistance as measured with 60-cycle alternating current was the same as the d.c. resistance, within the precision of measurement.

The data are collected in Fig. 8. The agreement between these results and those of Nagel and Wagner is good except at the lowest iodine pressures where Nagel and Wagner's conductivities are as much as 50 percent lower than those found in these experiments.

By interpolation, the conductivity of cuprous iodide as a function of iodine pressure for a cuprous-iodide temperature of 132.1°C, can be obtained from the data of Fig. 8. In conjunction with the results of Fig. 5, the conductivity as a function of the density of absorbed iodine atoms, can be plotted. This is done in Fig. 9. Over the range of excess iodine concentration investigated, the conductivity varies approximately as the 4/3 power of the density of the absorbed iodine atoms.

$$\sigma = \sigma_0 d^{4/3}. \tag{2}$$

DISCUSSION

Nagel and Wagner have proposed a mechanism for the absorption of iodine by cuprous iodide, similar to that which has been used, to successfully describe the behavior of cuprous oxide. They assume that two cuprous ions and two electrons wander to the surface of the solid for each iodine molecule absorbed. The result is an extension of the cuprous-iodide lattice, the formation of two vacancies in the cuprous ion lattice, and a defect of two electrons. This mechanism is plausible because the slight electrolytic conductivity of cuprous iodide is entirely due to the mobility of the Cu^+ ion. The reaction can be described by the chemical equation

$$2\,Cu^+ + I_2(g) \rightleftharpoons 2\,Cu^+ + 2I^- + 2V + 2h, \tag{3}$$

where the symbol, V, denotes a cuprous ion vacancy and the symbol, h, a defect of an electron or a "hole." The concentration of "holes" will then be proportional to the fourth root of the iodine vapor pressure, if the "holes"

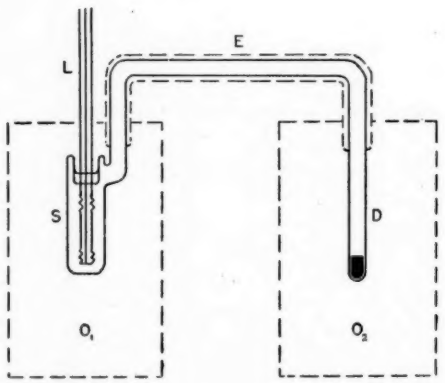

FIG. 7. Apparatus for determination of the electrical conductivity of cuprous iodide as a function of temperature and equilibrium vapor pressure of iodine.

are assumed free.

$$(h) = n = n_0 p_{I_2}^{\frac{1}{2}}. \tag{4}$$

Nagel and Wagner assume that the conductivity is proportional to the concentration of "holes," or

$$\sigma = \sigma_0 p_{I_2}^{\frac{1}{2}}. \tag{5}$$

This result is not in agreement with the experimental data of Fig. 8, although there is some indication that when the equilibrium vapor pressure is very small, Eq. (5) may be valid.

The conductivity of a semi-conductor is usually discussed in terms of Lorentz's equation:

$$\sigma = (4/3)[e^2 n l/(2\pi mkT)^{\frac{1}{2}}]. \tag{6}$$

The conductivity is proportional, at constant temperature, to the product of the density of charge carriers, n, and their mean free path, l. In Fig. 10, is shown the dependence of the mean free path, l, of the "holes" in cuprous iodide, upon the density of "holes." These data are calculated from the Hall effect and conductivity data of Steinberg.[6] If we assume that the density of "holes" is of the order of magnitude of the density of absorbed iodine atoms, the mean free path is a strong function of the density of "holes" for the range of densities involved in these experiments. In fact, the mean free path can be well respresented within this range, by the equation

$$l = l_0 n^{-0.3}. \tag{7}$$

If we assume that this relationship, obtained from Steinberg's measurements at room temperature, is valid at the higher temperature of the present experiments, we can combine (7) and (6) and conclude that

$$\sigma = (4/3)[e^2 l_0 n^{0.7}/(2\pi mkT)^{\frac{1}{2}}], \tag{8}$$

combining Eqs. (2) and (8), we have the result that, within the error of experiment, the density of conducting "holes" varies as the square of the density of absorbed iodine atoms,

$$n \propto d^2; \tag{9}$$

and is proportional to the equilibrium vapor pressure of iodine.

$$n \propto p_{I_2}. \tag{10}$$

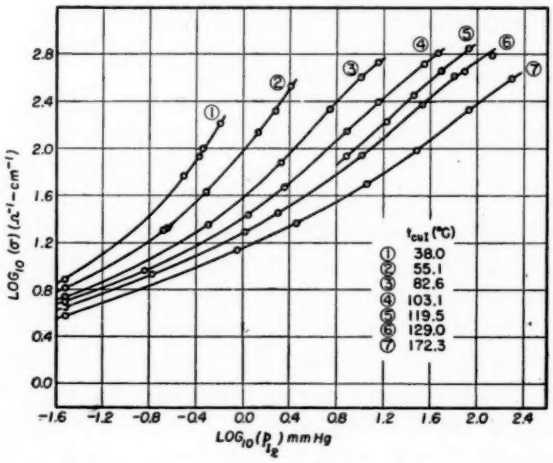

FIG. 8. The electrical conductivity of cuprous iodide as a function of temperature and equilibrium iodine pressure.

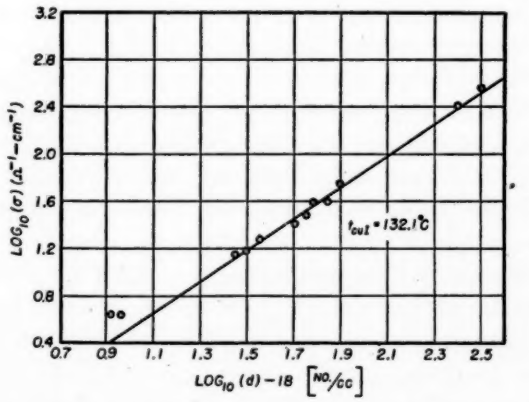

FIG. 9. The electrical conductivity of cuprous iodide as a function of the density of absorbed iodine atoms.

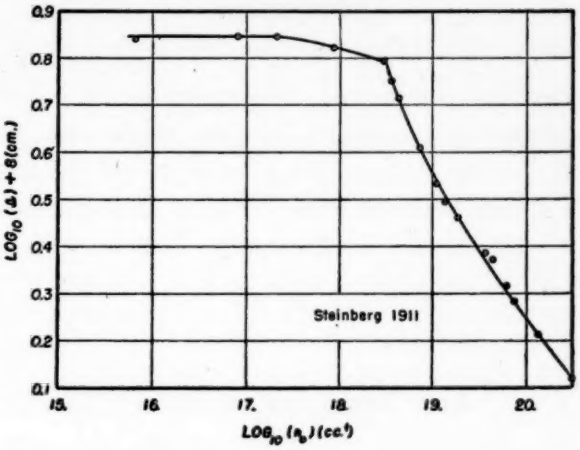

FIG. 10. The mean free path of the conducting "holes" in cuprous iodide as a function of the density of "holes." After Steinberg.

[6] K. Steinberg, Ann. d. Physik **35**, 1009 (1911).

CONCLUSION

The effect of the absorption of iodine upon the electrical conductivity of cuprous iodide is not adequately explained by the mechanism of Nagel and Wagner. We plan to extend the absorption measurements to other temperatures and to determine the Hall coefficient of cuprous iodide as a function of temperature and concentration of absorbed iodine.

The author is deeply indebted to Professor A. von Hippel, whose advice and assistance made possible the performance of the experiments described in this paper.

THE JOURNAL OF CHEMICAL PHYSICS VOLUME 13, NUMBER 8 AUGUST, 1945

Low Temperature Specific Heats of α-Manganese and γ-Manganese[1]

C. HOWARD SHOMATE[2]
Pacific Experiment Station, Bureau of Mines, United States Department of the Interior, Berkeley, California
(Received June 7, 1945)

The specific heats of α- and γ-manganese were measured in the temperature range 52° to 298°K. The specific heat curve of α-manganese exhibited a small "hump," extending over the temperature range 63°–103°K, with the peak of the "hump" occurring about 95°K. No anomaly appeared in the specific heat curve of γ-manganese. The computed heat contents and entropies per gram-atom are as follows: α-manganese, $H°_{298.16}-H°_0=1193\pm4$ cal., and $S°_{298.16}=7.59\pm0.04$ E.U.; γ-manganese, $H°_{298.16}-H°_0=1221\pm4$ cal., and $S°_{298.16}=7.72\pm0.04$ E.U.

A HIGH temperature allotropic modification of a metal seldom can be obtained in a sufficiently pure and stable form to determine its low temperature specific heat. Only one instance has been reported previously in the literature; *viz.*, gray tin.[3] γ-manganese which is stable at low temperatures has been prepared by a controlled electrolysis at the Salt Lake City Station of the Bureau of Mines. This paper presents low temperature specific heat data for this material and for α-manganese.

MATERIALS

The γ-manganese used in these measurements was prepared by David Schlain[4] by electrolysis of manganous sulfate in the absence of sulfites. In the presence of sulfites the electrolysis deposits α-manganese. The resistivity of each of forty-three strips of γ-manganese used in the measurements was determined by E. V. Potter.[5] The mean value was 45.1 microhms-cm, with a standard deviation of 0.4 microhms-cm. Previous measurements of other samples of γ-manganese showed resistivities of 42.8 ± 0.3, 45.6 ± 0.5, and 44.7 ± 0.2 microhms-cm. The resistivity of α-manganese is 185 microhms-cm. This is rather conclusive evidence of the absence of α-manganese in the γ-manganese sample; certainly it is not present to the extent of a few percent. The sample of γ-manganese was refrigerated immediately after preparation and, except for a few hours at room temperature, was kept refrigerated until the specific heat measurements were commenced. Indications are that the rate of conversion of γ- to α-manganese is very slow, even at room temperature. A 374.20-g sample of γ-manganese was used in the measurements.

After completion of the measurements on γ-manganese, the sample was removed from the calorimeter and conversion to α-manganese effected by heating gradually to 550°C in a high vacuum (10^{-4} mm Hg). Before conversion, the γ-manganese was ductile, but after conversion to α-manganese it became brittle. Specific heat measurements were then made on a 368.30-g sample of this α-manganese.

---

[1] Published by permission of the Director, Bureau of Mines, U. S. Department of the Interior.
[2] Chemist, Pacific Experiment Station, Bureau of Mines.
[3] F. Lange, Zeits. f. physik. Chemie **110**, 343 (1924).
[4] Metallurgist, Salt Lake City Station, Bureau of Mines.
[5] Physicist, Salt Lake City Station, Bureau of Mines.

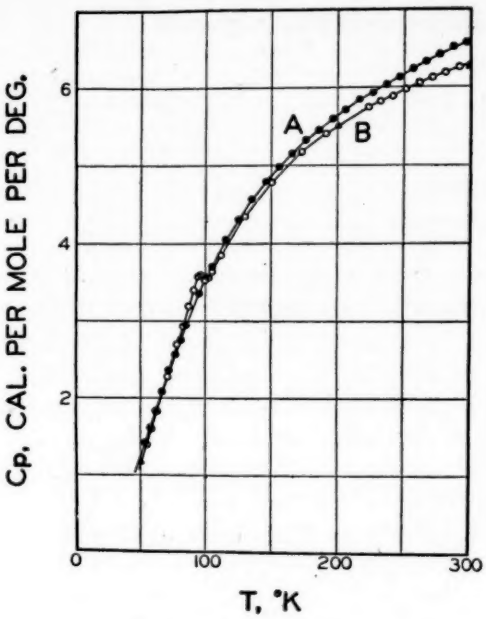

FIG. 1. Specific heats of γ-manganese (*A*), and α-manganese (*B*).

The dissolution of the sample of γ-manganese in $1N$ H_2SO_4 left a residue of 0.4 percent. In addition, it was possible to detect a slight odor of acetylenic hydrocarbons during the dissolution. It was felt that the best way to make corrections for these impurities was to make specific heat measurements of an available sample of very pure, electrolytic α-manganese prepared at the Bureau of Mines Station at Boulder City, Nevada.[6,7] The purity of this sample is purported to be at least 99.9 percent. It was degassed at 750°C in a high vacuum (10^{-4} mm Hg). The sample of this material used in the measurements weighed 484.61 g, and the specific heats are tabulated in Table I. The specific heat results for γ-manganese were corrected for impurities by assuming 1 percent impurities and correcting the results by a comparison of the specific heats of α-manganese prepared by conversion of γ-manganese and the Boulder City α-manganese. The corrections raise the specific heat values of the uncorrected γ-manganese about 0.2 percent on the average. If it had been assumed instead that the impurities were as low as 0.5 percent or as high as 2.0 percent, the corrected specific heat results would still be essentially the same as those obtained assuming 1.0 percent impurities. The corrected specific heat values of γ-manganese are also listed in Table I.

SPECIFIC HEATS

The method and apparatus used in the low temperature specific heat measurements have been described previously.[8,9] The experimental results in Table I are expressed in defined calories (1 calorie = 4.1833 international joules).[10] The results are represented graphically in Fig. 1. Values of the specific heats at 298.16°K, obtained by extrapolation of smooth curves through the experimental points, also are included in Table I. The atomic weights are in accordance with the 1941 International Atomic Weights. All weights were corrected to vacuum.

TABLE I. Specific heats of manganese (at. wt. = 54.93 g).

α-Manganese		γ-Manganese	
T, °K	C_p, cal./g-atom	*T*, °K	C_p, cal./g-atom
54.2	1.380	53.7	1.413
58.2	1.592	57.4	1.603
62.1	1.806	61.7	1.829
70.3	2.263	66.4	2.072
77.8	2.683	71.8	2.346
82.2	2.928	76.1	2.555
86.5	3.178	80.3	2.745
90.2	3.388	84.8	2.939
93.3	3.563	94.7	3.340
95.9	3.585	104.5	3.694
98.4	3.506	115.2	4.037
101.2	3.538	124.3	4.293
104.3	3.624	135.0	4.565
111.5	3.840	145.8	4.795
129.3	4.336	155.5	4.979
149.8	4.781	165.6	5.156
172.6	5.170	175.8	5.324
190.4	5.399	185.6	5.458
222.5	5.736	196.1	5.589
232.0	5.817	205.9	5.713
241.2	5 886	216.5	5.851
251.1	5.972	226.3	5.934
260.9	6.054	236.5	6.035
271.0	6.119	246.1	6.131
280.8	6.180	256.2	6.231
291.0	6.247	266.2	6.328
301.3	6.301	276.4	6.414
(298.16)	(6.29)	286.7	6.507
		296.3	6.568
		(298.16)	(6.59)

[6] R. S. Dean, Metals Technology **11**, No. 4, Technical Paper No. 1721 (1944), 17 pp.

[7] J. H. Jacobs, J. W. Hunter, W. H. Yarroll, P. E. Churchward, and R. G. Knickerbocker, Metals Technology **11**, No. 5, Technical Paper No. 1717 (1944), 21 pp.

[8] K. K. Kelley, J. Am. Chem. Soc. **63**, 1137 (1941).

[9] C. H. Shomate and K. K. Kelley, J. Am. Chem. Soc. **66**, 1490 (1944).

[10] E. F. Mueller and F. D. Rossini, Am. J. Phys. **12**, 1 (1944).

TABLE II. Heat contents and entropies at 298.16°K.

	α-Manganese		γ-Manganese	
	$H°-H_0°$, cal./g-atom	$S°$, E.U./g-atom	$H°-H_0°$, cal./g-atom	$S°$, E.U./g-atom
0°–52°K (extrap.)	18.3	0.48	18.9	0.49
52°–298.16°K (measured)	1175.	7.11	1202.	7.23
0°–298.16°K	1193.±4	7.59±0.04	1221.±4	7.72±0.04

The specific heat curve of γ-manganese showed no anomalies in the temperature range studied. However, a small "hump" appears in the specific heat curve of α-manganese, extending over the temperature range 63°–103°K, with the peak of the "hump" occurring about 95°K.

Kelley[11] reported low temperature specific heat data for α-manganese, which had been prepared by electrolyzing a solution containing manganous sulfate and ammonium sulfate into a mercury cathode and distilling the mercury from the resulting amalgam. The sample was a grayish powder consisting of clumps of particles of 4- to 5-microns average size. The low apparent density resulted in a sample size of only 112.53 g, which is less than one-fourth the size of the sample in the present measurements. In addition, oxide impurities corresponding to about 1 percent MnO were present. With these considerations the agreement of Kelley's work with the present measurements may be considered good. In general his results were about 0.3 percent higher. A few of Kelley's representative values have been plotted (black triangles) in Fig. 1.

Kelley did not report a "hump" in his specific heat curve of α-manganese. However, recalculation of his original data showed his specific heat value at 88.2°K to be in error. The corrected value is 3.251 cal./g-atom, or about 4 percent higher than the value of 3.130 cal./g-atom which he reported. Thus, re-examination of his specific heat curve indicated a "hump" of magnitude comparable to that in the present measurements.

HEAT CONTENTS AND ENTROPIES

The evaluation of the heat contents at 298.16°K is made by graphical integration from a plot of C_p against T, and entropies from a plot of C_p against log T. This necessitates extrapolation of the specific heat curves from the temperatures of the lowest measurements down to the absolute zero of temperature. The specific heat curves of α-manganese and γ-manganese were each fitted at the lower temperatures of the measurements by a single Debye function.

The values of θ in the Debye function, $D(\theta/T)$, were calculated for the α-manganese specific heat determinations at 54.2°, 58.2°, 62.1°, and 104.3°K to be 347.4, 348.0, 347.7, and 347.4, respectively. The values for intermediate determinations could not be used, since these specific heat values are affected by the "hump." The mean value is used to extrapolate the specific heat curve of α-manganese by the function, $D(347.6/T)$, yielding the extrapolated portion of the heat content, $H°_{52}-H°_0=18.3$ cal./g-atom, and of the entropy, $S°_{52}=0.48$ E.U./g-atom.

Evaluation of θ from the nine lowest temperature specific heat determinations of γ-manganese gave a mean value of $\theta=343.5\pm1.0$. The function, $D(343.5/T)$, gives the extrapolated values $H°_{52}-H°_0=18.9$ cal./g-atom, and $S°_{52}=0.49$ E.U./g-atom. Above 100°K the specific heat values of both α-manganese and γ-manganese begin to deviate from the Debye functions used in the extrapolations, the deviations becoming quite marked at higher temperatures.

The heat content and entropy associated with the "hump" in α-manganese was determined by summing the energies of eight successive specific heat determinations over the temperature range 80° to 106°K in the manner described by Shomate.[12] The excess energy in the "hump," above the specific heat curve represented by the function $D(347.6/T)$, is 4.72 cal./g-atom, and the excess entropy 0.054 E.U./g-atom.

Table II summarizes the heat content and entropy calculations for α- and γ-manganese.

[11] K. K. Kelley, J. Am. Chem. Soc. **61**, 203 (1939).

[12] C. H. Shomate, Ind. Eng. Chem. **36**, 910 (1944).

The Heat Content of Manganese at High Temperatures[1]

B. F. NAYLOR[2]
Pacific Experiment Station, Bureau of Mines, United States Department of the Interior, Berkeley, California

(Received June 7, 1945)

Heat contents above 298.16°K of two samples of electrolytic manganese were determined from room temperature to about 1440°K. From these data three transitions occurring at 1000±2°, 1374±5°, and 1410±5°K with heat effects of 535, 545, and 430 calories per gram-atom, respectively, were observed. Smooth curve values at 100° intervals and corresponding entropies are given as well as heat content and specific heat equations for the four modifications of manganese. A specific heat equation for γ-manganese was derived for the temperature range 298–1374°K from low temperature and high temperature thermal data; and corresponding heat contents and entropies above 298.16° for γ-manganese were calculated.

THE heat content of manganese at high temperatures and its transition points have been studied by numerous investigators,[3] but their data are inconsistent. This disagreement would appear to be due largely to lack of sample purity, resulting in sluggish transitions and thus producing erratic values. Heat content measurements, recently completed at this station, of two samples of pure electrolytic manganese gave results in good mutual agreement, from which the temperature and thermal magnitude of three transitions were determined.

TABLE I. Heat content of manganese (at. wt. = 54.93).

T, °K	$H_T - H_{298.16}$ (cal./g-atom)	T, °K	$H_T - H_{298.16}$ (cal./g-atom)	T, °K	$H_T - H_{298.16}$ (cal./g-atom)
		Sample A			
500.9	1406	993.5	5385	1354.2	9200
555.8	1822	999.2	5880	1355.6	9240
634.7	2378	1002.0	5980	1371.3	9595
648.8	2483	1025.9	6230	1373.6	9880
658.8	2563	1056.8	6490	1388.7	10,120
758.5	3374	1111.6	7010	1394.0	10,155
870.9	4328	1153.3	7375	1405.0	10,250
927.9	4809	1220.4	7975	1413.7	10,800
940.0	4917	1281.5	8525	1416.1	10,840
956.2	5060	1301.5	8725	1427.3	10,960
962.9	5125	1321.2	8945	1436.3	11,060
986.0	5300	1336.4	9075		
		Sample B			
366.9	469	1000.8	5605	1386.2	10,060
520.1	1558	1003.0	5990	1386.3	10,000
650.5	2515	1074.6	6620	1410.3	10,645
802.4	3683	1291.9	8585	1410.6	10,510
822.8	3867	1355.2	9260	1411.6	10,400
970.0	5155	1369.8	9490	1414.1	10,320
990.3	5330	1376.5	9840	1418.7	10,505
996.3	5485	1382.1	9950		

METHOD AND MATERIAL

The heat content measurements were made by the "drop" method in an apparatus previously described.[4] Frequent calibrations of the furnace thermocouple were made at the gold point in the manner outlined by Southard. The heat capacity of the copper calorimeter was determined electrically, the results being converted to the thermochemical calorie by the relation,[5] 1 cal. = 4.1833 int. joules (*NBS*). During the measurements the samples were enclosed in fused silica capsules filled with helium before sealing. The heat content of the capsule material was determined previous to the manganese measurements and closely checked values already reported[4, 6] for silica. Because of rapid devitrification of the silica above 900°C about 10 capsules were used during the course of the measurements and filled with an unused portion of manganese each time. The heat content of the silica contributed about 35 to 40 percent of the total heat evolved in the calorimeter.

The two electrolytic manganese samples were prepared at the Boulder City Station of the

[1] Published by permission of the Director, Bureau of Mines, U. S. Department of the Interior.

[2] Chemist, Pacific Experiment Station, Bureau of Mines.

[3] (*a*) J. C. Southard and C. H. Shomate, J. Am. Chem. Soc. **64**, 1770 (1942); (*b*) A. Sieverts and H. Moritz, Zeits. f. physik. Chemie **A180**, 249 (1937); (*c*) H. Yoshisaki, Sci. Rep. Tohoku Imp. Univ. **26**, 182 (1937); (*d*) L. V. Gayler, J. Iron Steel Inst. **115**, No. 1, 393 (1927); (*e*) S. Umino, Sci. Rep. Tohoku Imp. Univ. **16**, 775 (1927); (*f*) F. Wüst, A. Meuthen, and R. Durrer, Forsch. Arb. Ver. deut. Ing. No. 204 (1918); (*g*) R. Laemmel, Ann. d. Physik **16**, 551 (1905); (*h*) N. Stucker, Sitz. könig. Akad. Wiss. Wien **114**, 657 (1905).

[4] J. C. Southard, J. Am. Chem. Soc. **63**, 3142 (1941).

[5] E. F. Mueller and F. D. Rossini, Am. J. Phys. **12**, 1–7 (1944).

[6] W. P. White, Am. J. Sci. **47**, 1 (1919); J. Am. Chem. Soc. **55**, 1050 (1933).

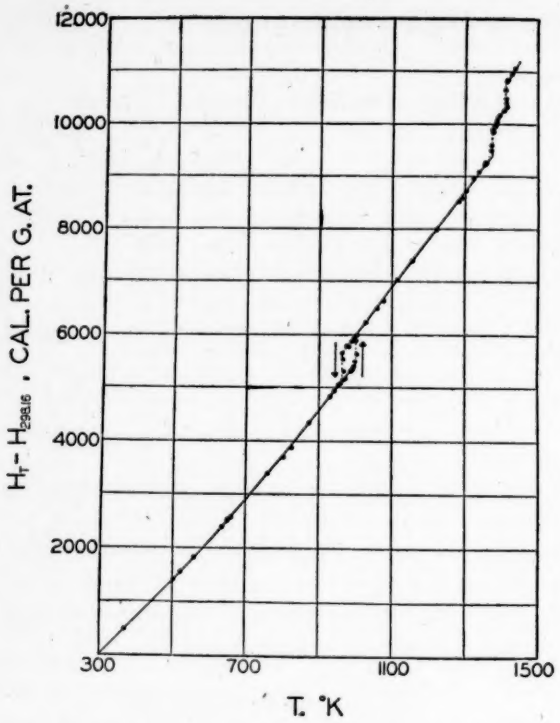

FIG. 1. High temperature heat contents of manganese above 298.16°K.

Bureau of Mines and were at least 99.9 percent pure after degassing free of hydrogen. Sample *A* was degassed by heating to 850°C in a vacuum of 10^{-5} mm and allowed to cool slowly. Sample *B* was treated similarly at 900°C. Although the impurities present in each sample are very small, sample *A* was considered the purer, as it was free of silicon while sample *B* contained 0.03 percent.

RESULTS

Experimental heat contents above 298.16°K are given in Table I for both samples *A* and *B*. Except for several low points in the β-range, the results of the two samples are in good agreement. From the data, the existence of three transition points in the range 298°–1436°K is readily discernible. These transitions, as well as the experimental points, are shown in Fig. 1. The listing arrangement in Table I does not necessarily conform with the experimental order; in fact, many of the determinations at lower temperatures followed those at higher temperatures.

It was assumed that the manganese came to the same final state (alpha) in the calorimeter, regardless of its temperature before cooling. For all determinations in Table I within 50° of the $\alpha \rightarrow \beta$ transition point, the furnace was brought to thermal equilibrium; the capsule was then admitted and, upon reaching furnace temperature, was dropped into the calorimeter. Thus the capsule always was heating before dropping. This procedure was followed upon finding that β-manganese could be readily supercooled. Such sluggishness was not noticed in the transitions at higher temperatures.

Series of measurements, made to observe the extent to which β-manganese could be supercooled, are arranged in Table II in the order of determination. These involved heating the sample to at least 1010°K within the furnace, cooling the furnace as rapidly as possible to the run temperature, bringing it to equilibrium, and then proceeding to drop the sample as usual. The cooling process required about 20 to 30 minutes. It was found that β-manganese could be supercooled to 960°±10°K. Under faster cooling conditions a reduction of this value might be achieved.

The transition points and associated heat effects obtained from the data given in Table I are tabulated in Table III.

Smooth curve values at 100° intervals and corresponding graphically computed entropies are listed in Table IV. Heat content equations representing the experimental data have been derived and are given below. They are based on the fol-

TABLE II. Heat content of supercooled β-manganese (at. wt. = 54.93).

T, °K	$H_T - H_{298.16}$ (cal./g-atom)	T, °K	$H_T - H_{298.16}$ (cal./g-atom)
Sample A		Sample B	
972.9	5770	997.2	5880
961.8	5640	994.2	5915
950.6	5030	987.4	5860
		979.2	5770
		967.6	5295
		963.0	5520

TABLE III.

Transition	T, °K	Heat of trans. (cal./g-atom)
$\alpha \rightarrow \beta$	1000±2	535
$\beta \rightarrow \gamma$	1374±5	545
$\gamma \rightarrow \delta$	1410±5	430

lowing values: α-manganese, $C_{p\ 298.16}=6.29$,[7] $H_T-H_{298.16}=2895$ and 5450 cal. at 700° and 1000°K; β-manganese, $H_T-H_{298.16}=5985$, 7795, and 9395 cal. at 1000°, 1200°, and 1374°K; γ-manganese, $H_T=H_{298.16}=9940$ and 10,330 cal. at 1374° and 1410°K; δ-manganese, $H_T-H_{298.16}=10{,}760$ and 11,210 cal. at 1410° and 1450°K, respectively.

The appropriate temperature range and the mean percentage deviation of the equation from the experimental data are given after each equation.

$$\text{Mn}(\alpha): H_T-H_{298.16}=5.70T+0.00169T^2+(37{,}500/T)-1975(298°\text{–}1000°\text{K};\ 1\%),$$

$$\text{Mn}(\beta): H_T-H_{298.16}=8.33T+0.00033T^2-2675(1000°\text{–}1374°\text{K};\ 0.2\%),$$

$$\text{Mn}(\gamma): H_T-H_{298.16}=10.70T-4760(1374\text{–}1410°\text{K};\ 0.1\%),$$

$$\text{Mn}(\delta): H_T-H_{298.16}=11.30T-5170(1410°\text{–}1450°\text{K};\ 0.0\%).$$

Differentiating the above heat content equations gives the corresponding specific heat relationships.

$$\text{Mn}(\alpha): C_p=5.70+0.00338T-(37{,}500/T^2),$$
$$\text{Mn}(\beta): C_p=8.33+0.00066T,$$
$$\text{Mn}(\gamma): C_p=10.70,$$
$$\text{Mn}(\delta): C_p=11.30.$$

DISCUSSION

Heat content data for manganese comparable to this work were reported by Southard[3a] and by Wüst and co-workers.[3b] Southard's results are somewhat lower except around 650°K where they are in good agreement. From 800°K to the $\alpha\rightarrow\beta$ transition the difference is about 2 percent, thus reducing the heat of transition in the present instance to 535 calories. In the β-range there is fair agreement if the 65-calorie correction, advocated by Southard, is added to his values. The values of Wüst are lower than the present work by only 1 to 2 percent below 1000°K but are in complete disagreement above that temperature, since no perceptible $\alpha\rightarrow\beta$ transition was found.

TABLE IV. Heat content and entropy.

T, °K	$H_T-H_{298.16}$ (cal./g-atom)	$S_T-S_{298.16}$ (cal./deg./g-atom)
400	690	1.99
500	1385	3.54
600	2120	4.88
700	2895	6.07
800	3715	7.16
900	4570	8.17
1000	5450 (α)	9.10
1000	5985 (β)	9.63
1100	6890	10.50
1200	7795	11.28
1300	8715	12.02
1374	9395 (β)	12.53
1374	9940 (γ)	12.93
1400	10,220	13.13
1410	10,330 (γ)	13.21
1410	10,760 (δ)	13.51
1450	11,210	13.83

[7] C. H. Shomate, J. Chem. Phys. **13**, 326 (1945).

TABLE V. Heat content and entropy of γ-manganese.

T, °K	$H_T-H_{298.16}$ (cal./g-atom)	$S_T-S_{298.16}$ (cal./deg./g-atom)
400	705	2.02
500	1445	3.68
600	2230	5.10
700	3050	6.37
800	3915	7.52
900	4815	8.58
1000	5750	9.57
1100	6720	10.50
1200	7730	11.38
1300	8780	12.21
1374	9570	12.80

The present data for manganese are considered more reliable and complete than any previously reported. Besides having samples of exceptional purity, several refinements in the apparatus were made since Southard's work, and considerably more effort was expended to isolate and investigate the transitions, especially those occurring at higher temperatures. That a fourth modification (delta) of manganese does exist is shown conclusively by the present data.

The herein reported transition temperatures have been checked within a few degrees at the Salt Lake City Station of the Bureau of Mines by thermal-analysis and hydrogen-solubility measurements. The $\alpha\rightarrow\beta$ transition also was observed to be sluggish, its temperature depending on whether the sample was heating or cooling at the time of measurement. Hence, some doubt exists as to the true equilibrium temperature. However, for purposes of making thermodynamic calculations, 1000°K was selected; admittedly this may produce some error, but it is negligible except near or at the transition temperature.

Gamma-manganese is found often as a separate phase in manganese alloys, but is thermodynamically unstable in the pure state below 1374°K. However, low temperature specific heats have been determined,[7] as at temperatures less than 273°K its rate of transformation is very low. Transformation occurs almost instantaneously around 398°K; hence no heat contents can be measured between room temperature and 1374°K. Knowing the total virtual entropy of γ-manganese at 1374°K to be the same regardless of its origin, a specific heat equation for γ-manganese was derived, using the data:

(γ-Mn), $C_{p\ 298.16}=6.59$, $(dC_p/dT)_{298.16}=0.0069$,

and

$S_{298.16}=7.72$; (α-Mn), $S_{298.16}=7.59$;

and

$$S_{1374}(\gamma\text{-Mn})-S_{298.16}(\alpha\text{-Mn})=12.93,$$
$$C_p=6.03+0.00356T-(44{,}300/T^2).$$

Integrating gives

$$H_T-H_{298.16}=6.03T+0.00178T^2+(44{,}300/T)-2105,$$

where $H_T-H_{298.16}$ represents the heat liberated in calories per gram-atom in cooling γ-manganese from T°K to produce γ-manganese at 298.16°K. Heat content values, calculated from this equation, and entropies, obtained by integration, are given in Table V at 100° intervals to 1374°K.

THE JOURNAL OF CHEMICAL PHYSICS VOLUME 13, NUMBER 8 AUGUST, 1945

Rate-Dependent Chromatographic Adsorption

JOHN E. WALTER
Palmer Physical Laboratory, Princeton University, Princeton, New Jersey

(Received May 25, 1945)

The process of chromatographic adsorption is studied from the kinetic viewpoint, assuming a bimolecular reaction between adsorbent and solute. Boundaries characteristic of equilibrium adsorption are obtained only if the time of passage of the solution through the column is greater than the half-life of the reaction by a factor of at least one hundred.

INTRODUCTION

In a recent article[1] the author presented the results to be expected if one or more solutes are adsorbed by a chromatographic process, assuming the adsorption isotherm to be the equilibrium equation for a bimolecular chemical reaction. The distribution of adsorbed solute along the adsorbing column was found to be a definite function of the equilibrium constants of the reactions. In this article the same process is investigated from the kinetic viewpoint in order to see how the previous results are modified if equilibrium is not attained.

We assume the adsorption to be represented by a bimolecular reaction of the type

$$\underset{(P-Q)}{HZ}+\underset{(C)}{MX}\rightleftharpoons\underset{(Q)}{MZ}+\underset{(C^0-C)}{HX}, \qquad (1)$$

where (C) is the concentration of the solute in solution, (Q) is the concentration of adsorbed solute, (P) is the capacity per unit length of the tube, and (C^0) is the original concentration of the solute. If l is the distance down the tube and v is the volume of solution which has passed the point l, we have

$$\partial Q/\partial v+\partial C/\partial l=0, \qquad (2)$$

as the equation of continuity. If θ is the time during which the solution has been in contact with the adsorbing material at a given position along the tube, we have

$$\partial Q/\partial\theta=k_f C(P-Q)-k_b Q(C^0-C), \qquad (3)$$

where k_f and k_b are the rate constants for the forward and backward reactions in (1). If R is the rate at which the solution is passed through the tube, we have

$$\partial Q/\partial\theta=(\partial v/\partial\theta)(\partial Q/\partial v)=R\partial Q/\partial v, \qquad (4)$$

[1] J. Walter, J. Chem. Phys. **13**, 229 (1945).

and Eq. (3) becomes

$$R\partial Q/\partial v = k_f C(P-Q) - k_b Q(C^0 - C). \quad (5)$$

Placing $R=0$ gives the equilibrium relation between C and Q, and the problem reduces to that previously treated. Eliminating C from Eqs. (2) and (5) leads to

$$[k_f P + (k_b - k_f)Q]^2(\partial Q/\partial v) + k_f k_b C^0 P(\partial Q/\partial l) + R\left\{[k_f P + (k_b - k_f)Q]\frac{\partial^2 Q}{\partial v \partial l} - (k_b - k_f)\frac{\partial Q}{\partial v}\frac{\partial Q}{\partial l}\right\} = 0, \quad (6)$$

as the differential equation governing the distribution of Q along the adsorbing column. The boundary conditions are $Q=0$ for $v=0$ and $C=C^0$ at $l=0$. This last condition implies

$$R\partial Q/\partial v = k_f C^0(P-Q); \quad l=0, \quad v \geqq 0, \quad (7)$$

or

$$Q = P\{1-\exp[-k_f C^0 v/R]\}; \quad l=0. \quad (8)$$

As a subsidiary condition which can be used as a check, we have

$$\int_0^\infty Q dl = C^0 v, \quad (9)$$

expressing the conservation of solute. The substitutions

$$q = Q/P, \quad v = Rt/C^0 k_f, \quad l = Rx/Pk_f, \quad (10)$$

reduce the equations to

$$[k_f + (k_b - k_f)q]^2\frac{\partial q}{\partial t} + k_b k_f \frac{\partial q}{\partial x} + k_f[k_f + (k_b - k_f)q]\frac{\partial^2 q}{\partial x \partial t} - k_f(k_b - k_f)\frac{\partial q}{\partial t}\frac{\partial q}{\partial x} = 0; \quad (11)$$

$$q = 1 - e^{-t}; \quad x = 0; \quad (12)$$

$$\int_0^\infty q dx = t. \quad (13)$$

Equation (11) can be solved exactly for $k_b=0$ and for $k_b=k_f$, although the latter solution cannot be given in closed form. The author has not succeeded in obtaining an exact solution for the general problem, but for the interesting case $k_b > k_f$ an approximate solution, valid for large values of t, is presented.

$k_b = 0$

For $k_b=0$, the term in (11) involving $\partial q/\partial x$ drops out of the equation, which can then be rearranged to give

$$(1-q)^2\frac{\partial}{\partial t}\left\{q + \frac{1}{1-q}\frac{\partial q}{\partial x}\right\} = 0, \quad (14)$$

so that either $q=1$ or

$$q + [1/(1-q)](\partial q/\partial x) = f(x), \quad (15)$$

where $f(x)$ is an arbitrary function of x. The boundary conditions can be satisfied by placing $f(x)=0$. We then have

$$q/(1-q) = g(t)e^{-x}, \quad (16)$$

where $g(t)$ is an arbitrary function of t. From (12) we find

$$q/(1-q) = (e^t - 1)e^{-x}. \quad (17)$$

This solution satisfies Eq. (13), and thus justifies the choice $f(x)=0$.

The distribution represented by (17) is illustrated in Fig. 1 for several values of t. Variations in t are considered here to mean variations in R. For $t=1$, the adsorbing material at the end of the tube is about 63 percent saturated after the given volume has passed. It will be noted that only for $t>100$ do we obtain a close approxima-

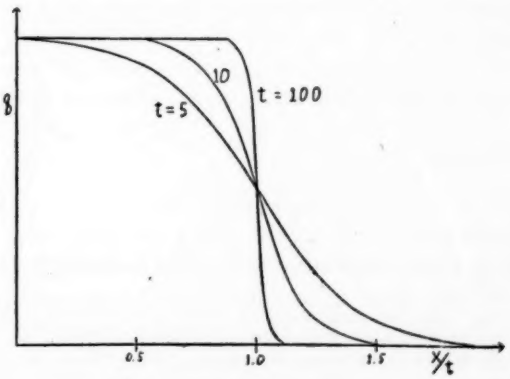

FIG. 1. Distribution for $k_b=0$.

tion to the discontinuous adsorption predicted by the equilibrium theory; that is, only if the time of passage of the solution is of the order of 100 times the "half-life" of the chemical reaction.

$$k_b = k_f$$

For $k_b = k_f$, corresponding to an equilibrium constant of unity for the reaction, Eq. (11) reduces to the linear form

$$\partial q/\partial t + \partial q/\partial x + \partial^2 q/\partial x \partial t = 0. \tag{18}$$

There are no difficulties involved in writing down general solutions for this equation, but

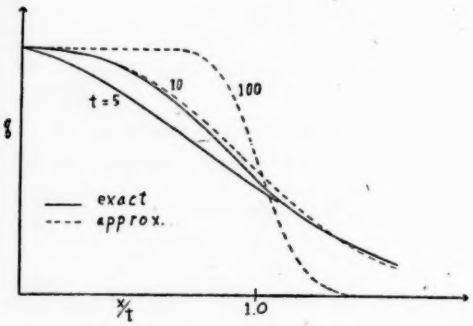

FIG. 2. Distribution for $k_b = k_f$.

fitting the boundary conditions is a less trivial matter. For this reason the Laplace transformation was employed.[2] By the substitution

$$q = e^{-t-x} F(t, x), \tag{19}$$

the equation is reduced to

$$\partial^2 F/\partial x \partial t - F = 0, \tag{20}$$

which leads to a tabulated inverse transform. If we let $f(s, x)$ be the transform of $F(t, x)$ with respect to the variable t, the transformed problem becomes

$$s\partial f/\partial x - f = 0; \quad f(s, 0) = 1/s(s-1), \tag{21}$$

which leads to

$$f(s, x) = e^{x/s}/s(s-1). \tag{22}$$

The inverse transform of $e^{x/s}/s$ is $I_0\{2(xt)^{\frac{1}{2}}\}$ where I_0 is the Bessel function

$$I_0\{2(xt)^{\frac{1}{2}}\} = 1 + xt + (x^2t^2/[2!]^2) + \cdots. \tag{23}$$

The inverse transform of $f(s, x)$ is therefore

$$F(t, x) = \int_0^t e^{t-\tau} I_0\{2(x\tau)^{\frac{1}{2}}\} d\tau. \tag{24}$$

It can be verified without difficulty that the solution represented by (19) and (24) satisfies all the boundary conditions. This solution can be given in series form as

$$q = e^{-t-x} \sum_{n=0}^{\infty} \left\{ \sum_{n+1}^{\infty} \frac{t^m}{m!} \right\} \frac{x^n}{n!} \tag{25}$$

$$= 1 - e^{-t-x} \sum_{n=0}^{\infty} \left\{ \sum_{m=0}^{n} \frac{t^m}{m!} \right\} \frac{x^n}{n!}. \tag{26}$$

Figure 2 includes curves calculated from these series for $t=5$ and $t=10$. For larger values of t, a satisfactory asymptotic solution can be found. We write (19) as

$$q = 1 - e^{-x} \int_t^{\infty} e^{-\tau} I_0\{2(x\tau)^{\frac{1}{2}}\} d\tau. \tag{27}$$

Now for large values of the argument, I_0 becomes equal to

$$I_0\{2(x\tau)^{\frac{1}{2}}\} = \frac{1}{2\pi^{\frac{1}{2}}} \frac{1}{(x\tau)^{\frac{1}{4}}} \exp[2(x\tau)^{\frac{1}{2}}]; \quad x\tau \to \infty. \tag{28}$$

With this approximation to I_0, q can be written as

$$q = 1 - \frac{1}{2\pi^{\frac{1}{2}}} \int_t^{\infty} \left(\frac{\tau}{x}\right)^{\frac{1}{4}} \frac{\exp[-(x^{\frac{1}{2}} - \tau^{\frac{1}{2}})^2]}{\tau^{\frac{1}{2}}} d\tau. \tag{29}$$

Aside from the factor $\tau^{\frac{1}{4}}$, this integral has the form of the probability integral or error function. Since this factor is a slowly varying function, we will remove it from the integrand. For $t<x$, the integrand has its maximum value at $\tau = x$; for $t>x$, the integrand has its maximum value at $\tau = t$. Using these values for τ when we remove $\tau^{\frac{1}{4}}$ from the integrand, we obtain

$$q = 1 - \tfrac{1}{2}(t/x)^{\frac{1}{4}}\{1 - \text{erf}\,(t^{\frac{1}{2}} - x^{\frac{1}{2}})\}; \quad x < t, \tag{30}$$

$$q = 1 - \tfrac{1}{2}\{1 + \text{erf}\,(x^{\frac{1}{2}} - t^{\frac{1}{2}})\}; \quad x > t, \tag{31}$$

[2] The notation used here is that of R. V. Churchill, *Modern Operational Mathematics in Engineering* (McGraw-Hill Book Company, Inc., New York, 1944). The necessary theorems and the appropriate function-transform pairs will be found in this text.

where erf (z) is the error function

$$\text{erf}\,(z)=\frac{2}{\pi^{\frac{1}{2}}}\int_0^z \exp\,(-\alpha^2)d\alpha, \qquad (32)$$

which is a tabulated function. For $t=10$, Eqs (30) and (31) are nearly correct, as indicated in Fig. 2, and will of course be more accurate for larger values of t. For very large values of t, Eqs. (30) and (31) can be replaced by

$$q=\tfrac{1}{2}+\tfrac{1}{2}\,\text{erf}\,(t^{\frac{1}{2}}-x^{\frac{1}{2}}) \qquad (33)$$

because the variation in $(t/x)^{\frac{1}{2}}$ is not significant in the region of interest. Figure 2 includes the curve for $t=100$; Eqs. (33), (30), and (31) give nearly identical results in this range. It will be noted that this approximate result (33) satisfies the differential equation exactly. It does not satisfy the conservation condition exactly, but does so to a good approximation. The distribution for $k_b=k_f$ is similar to that for $k_b=0$, but the cut-off is considerably less sharp for the same value of t. In the equilibrium case, the adsorption is discontinuous for the entire range $k_b<k_f$. No further new qualitative effects are to be expected in this range.

$k_b>k_f$

For $k_b>k_f$, the boundary of the adsorbed material is not sharp even under equilibrium conditions. The differential equation for this range is

$$[1+\beta q]^2\frac{\partial q}{\partial t}+\frac{1}{K}\frac{\partial q}{\partial x}+[1+\beta q]^2\frac{\partial}{\partial x}\frac{1}{1+\beta q}\frac{\partial q}{\partial t}=0, \qquad (34)$$

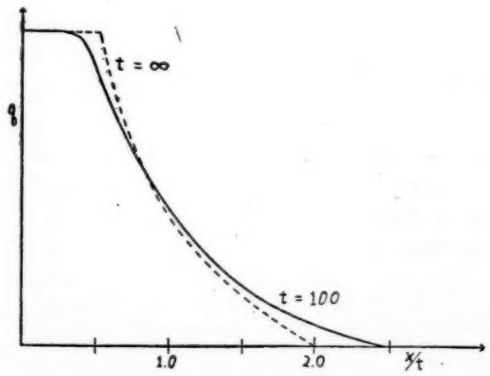

FIG. 3. Distribution for $K=0.5$.

where $K=k_f/k_b$, $\beta=(1-K)/K$. We suggest as an approximate solution, valid for large t,

$$q=\tfrac{1}{2}+\tfrac{1}{2}\,\text{erf}\,(z),$$
$$z=\{t/K(1+\beta q)\}^{\frac{1}{2}}-\{(1+\beta q)x\}^{\frac{1}{2}}. \qquad (35)$$

This solution was suggested by the fact that, if the quantity $(1+\beta q)$ were a constant, (35) would be a solution of Eq. (34). Using (35) we find that the first two terms in (34) are of the order $t^{-\frac{1}{2}}$ and $x^{-\frac{1}{2}}$, respectively; the last term is of the order $(xt)^{-\frac{1}{2}}$. The first two terms in (34) combine to give a term of the order $(xt)^{-\frac{1}{2}}$, which is cancelled by a term from the second derivatives. Equation (35) therefore satisfies the differential equation asymptotically as $xt\to\infty$. Also, as $t\to\infty$, (35) gives the correct equilibrium distribution

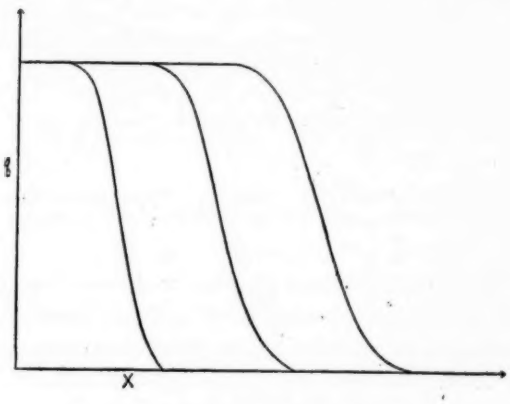

FIG. 4. Moving boundary for $K=1.0$.

$$(1+\beta q)^2=t/Kx; \quad Kt<x<t/K. \qquad (36)$$

Equation (35) satisfies the boundary conditions to a good approximation for large values of t. It is not, however, to be expected that the results given by (35) are more than qualitatively correct. Figure 3 represents the distribution calculated from Eq. (35) for $t=100$, $K=0.5$.

CONCLUSION

The two curves in Fig. 3 do not appear at first glance to differ significantly. However, the solid curve actually resembles very closely the equilibrium curve for $K=0.4$. This indicates that the use of the distribution curve for the determination of equilibrium constants may give

quite inaccurate results unless the solution is passed through the column very slowly. Similarly, the curve for $t=100$ in Fig. 2 resembles the equilibrium curve for a K of about 0.8 rather than unity.

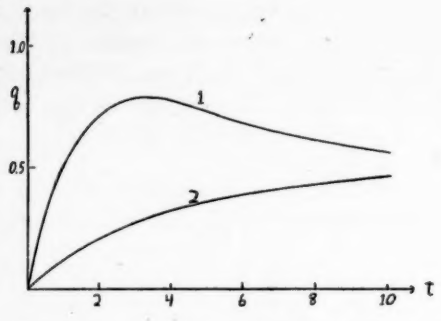

FIG. 5. Distribution at $x=0$ for two components with equal equilibrium constants but different rate constants.

Variations in t can also be considered as variations in v at constant R. The above results can therefore be used to see how the adsorption pattern changes as it progresses down the column. For $k_b=0$, we find that the boundary remains constant in width as it progresses down the column. For $k_b>0$, the boundary becomes less sharp as it moves along. Figure 4 illustrates this behavior for $k_f=k_b$. The successive curves are calculated for $t=50$, 100, 150; R is assumed to be constant.

It is not probable that much useful information can be obtained by studying the rate equations for multiple adsorption. For small values of R, we would expect simply a blurring of the equilibrium patterns. For large values of R, there exists of course a possibility of separating two solutes which have the same equilibrium constants but different rate constants. Some information on this problem can be obtained by investigating the variations in the concentration of the adsorbed material at the entrance end of the tube. This is a standard problem, so the algebraic results will not be repeated here, but a curve might be of interest in connection with the previous results. Figure 5 represents the variation in the concentrations of the adsorbed material at $l=0$. The solutes are assumed to be present in the solution in equal concentrations, and the two equilibrium constants are assumed to be equal. The forward rate constant for solute 1 is assumed to be ten times that of solute 2. The parameter t is the same as that used previously, except that the average value of the forward rate constants replaces the forward rate constant for the single reaction. For this particular situation, we note that if the solution is passed through the tube at a rate corresponding to $t>10$, we will have essentially the equilibrium distribution, that is, no appreciable separation of the two components. However, if the solution is passed through the tube at a more rapid rate corresponding to $t=2$, component 1 will be largely adsorbed at the beginning of the tube, and an appreciable separation will have been obtained.

Phenomenological Theory of Emulsion Polymerization

ELLIOTT W. MONTROLL
Department of Chemistry, Polytechnic Institute of Brooklyn, Brooklyn, New York
(Received April 2, 1945)

The process of emulsion polymerization is observed to occur in the following manner. An aqueous emulsion of monomer is prepared using a soap as the emulsifier. The addition of a catalyst starts the polymerization after an initiation period whose length depends on the mean radius of the monomer globules (long periods for large mean radius and short periods for small mean radius). As the reaction proceeds, the mean radius of the globules diminishes and the free soap concentration increases. It is believed that the initiation period is the result of the existence of an inhibitor in the monomer. The catalyst reacts with that part of the inhibitor which is dissolved in the water phase, so that in order for equilibrium to be restored some of the inhibitor must diffuse out of the monomer. Rate curves are derived on this basis using the added assumptions: (a) polymerization occurs at the monomer-water interface after the inhibitor concentration has reached a low threshold value. (b) radius distribution function of monomer has a single maximum.

A. INTRODUCTION

CONSIDERABLE theoretical and experimental work has been done on the mechanism of polymerization in *homogeneous* systems, such as pure liquids or solutions; and it has been possible to express the course of such reactions with fair approximation by a set of equations which represent the different cooperating elementary steps of the whole process, such as activation, propagation, chain transfer, termination, etc. Recently, polymerization in heterogeneous systems, such as emulsions and suspensions, has become of considerable practical importance; and a somewhat detailed study of the fundamental background of such processes appears, therefore, to be of interest. Only few papers (all of them very recent) report experimental facts about emulsion and suspension polymerization,[1] but none of them makes an attempt at a qualitative theoretical analysis.

This article intends to show how, under given assumptions, the case of polymerization in emulsion can be treated mathematically. It involves such simultaneous processes as diffusion, solubilization, and chemical reaction, which take place in different parts of the system and together determine the rate of conversion of the monomer into the polymer. It is evident that different kinds of assumptions can be made regarding the locations of the various elementary steps, and it is to be expected that at the present incomplete state of our experimental knowledge the special assumptions made in this paper will require revision and improvements. But it can be hoped that the general mathematical procedure will, with certain modifications, be useful and applicable after more reliable experimental data are available.

Let us, therefore, consider the polymerization of styrene in aqueous emulsion. The conditions are, in general, the following: About 20 ml monostyrene are added to 180 ml water, which contains about 1 gram soap (ammonium oleate) and with the aid of moderate shaking, a stable emulsion of monostyrene in water is produced. Previous observations and measurements[2] have

TABLE I. Distribution of particle size. (From Clayton's data, reference 3.)

Soap concentration	% 2.0–2.5μ	% 2.5–3.0μ	% 3.0–3.5μ	% 3.5–4.0μ	% 4.0–4.5μ	% 4.5–5.0μ	% 5.0–5.5μ	% 5.5–6.0μ
0.0005M	—	—	—	14	23	31	18	9
0.0010	—	—	5	22	34	23	6	6
0.0015	—	5	22	20	30	14	9	—
0.0020	—	18	24	29	18	11	—	—
0.0025	6	29	39	13	12	3	—	—

[1] Fryling and Harrington, Ind. Eng. Chem. **36**, 114 (1944); J. R. Vinograd, L. L. Fong, and W. M. Sawyer: Abstracts of the papers presented at the ACS Meeting in New York City, September 1944, page 3E; W. P. Hohenstein, S. Siggia, and H. Mark, India Rubber World **111**, 173 (1944); **112**, 436 (1945).

[2] Compare W. Clayton, reference 3; S. Berkman and G. Egloff, *Emulsions and Foams* (Reinhold Publishing Company, New York, 1944); and particularly J. W. McBain.

shown that in such cases a multitude of small hydrocarbon droplets are formed, the radii of which cover a wide range and exhibit average values in the neighborhood of one micron. The average particle diameter and the distribution

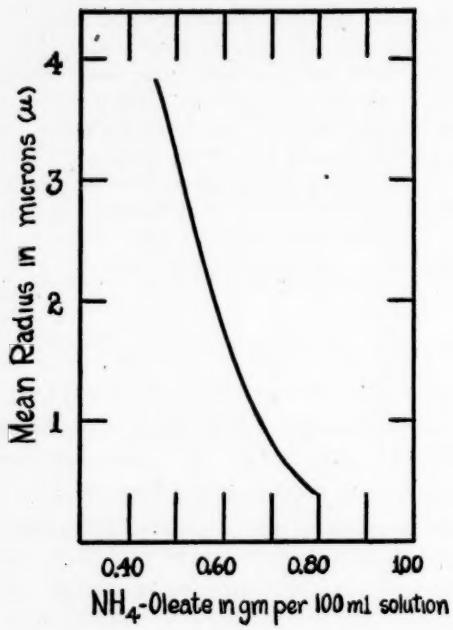

FIG. 1. Variation of mean globule radius of an emulsion as a function of emulsifier concentration.

curve depend upon various parameters, such as temperature, mode and vigor of shaking, and particularly upon the ratio hydrocarbon (monostyrene) to soap solution (concentration of soap and total volume of aqueous phase). Table I shows as an example a few rough particle size distribution functions[3]; and Fig. 1 shows how, in the case of monostyrene emulsions, the average radius of the dispersed particles depends upon the soap concentration, while the ratio of hydrocarbon phase to aqueous phase is kept constant[1] (1:10).

These results are commonly explained by assuming that those soap molecules which are not incorporated in either type of soap micells (laminar molecular micells and spherical ionic micells), but are monomolecularly distributed in the aqueous phase, either as undissociated (neutral) acid molecules or as dissociated soap and sodium ions, are adsorbed on the surface of the hydrocarbon (monostyrene) globules. The long ($C_{12}-C_{20}$) hydrocarbon chain of the fatty acid (ion or molecule) is soluble in the hydrocarbon of the dispersed particles, while the COOH, COONa or COO^- groups are highly polar and therefore preponderantly attracted by the aqueous phase.

Emulsions of this nature are used to carry out polymerization. The reaction is initiated by a water soluble substance of peroxide nature called the "catalyst." In most experiments reported in the literature, sodium or ammonium persulfate, perborate, or percarbonate have been used. Upon addition of the "catalyst" and continuous agitation of the system, reaction does not set in at once, but one always observes a shorter or longer inhibition period during which practically no polymer is formed, but some of the "catalyst" is used up. This fact is usually explained by assuming that certain dissolved impurities in the monomer phase or in the water inhibit the formation of long chains and must be destroyed before polymerization can effectively set in. The temperature range in which such reactions are carried out is usually between 40° and 80°C.

Three zones of reaction are possible: 1. in the monostyrene phase, 2. in the water phase, and 3. at the styrene-water interface.

Since the catalysts used in styrene polymerization are generally inorganic salts insoluble in styrene, it is highly improbable that the reaction could occur inside the styrene globules. If the reaction zone were in the aqueous phase, the rate should be independent of total interface surface, which does not seem to be the case. When the reaction zone is at the water-styrene interface, the change in volume of a styrene globule is proportional to the surface area of the globule, or

$$dV/dt = -4\pi kr^2,$$

where k is the proportionality constant. Since the sphere volume is given by $V=4\pi r^3/3$, this leads to $dr/dt=-k$, and the radius diminishes at a constant rate. This law of disappearance of monomer was observed (microscopically) in soap solutions of many organic liquids, including styrene, by Vinograd, Fong, and Sawyer. In this paper we shall consider only those reactions which occur at the interface.

[3] Compare W. Clayton, *Theory of Emulsions and Their Technical Treatment* (The Blakiston Company, Philadelphia, Pennsylvania, 1938), fourth edition, p. 132.

The rate at which monomer is polymerized in a stable emulsion depends on the initial size distribution of the suspended globules and on the state of agitation of the system. We shall devote our attention to initial radius distributions with a single maximum, and to reactions which proceed while the system is in a state of constant agitation. In reactions occurring under these conditions one would expect the radius distribution curve of monomer spheres to have a single maximum at all times.

In Fig. 2 are plotted experimental curves determined by Siggia,[1] Hohenstein, and Mark, showing the rate of polymerization of monostyrene when ammonium oleate is used as an emulsifier and the reaction is catalyzed by sodium perborate. The polymerization was carried out in a shaker with 78 shakings per minute. The curves from right to left correspond to initial distributions having decreasing mean radii. Two interesting features of these curves are: 1. The inhibition period increases with the initial mean radius, and 2. The rate curves are essentially parallel in the range of intermediate degrees of polymerization.

Unfortunately the nature and concentration of the inhibitor were not determined in these experiments.

Using the properties of monostyrene-water emulsions given so far, we shall now discuss a polymerization mechanism which qualitatively accounts for the curves given in Fig. 2. First[4] a process leading to an inhibition period which increases with the initial mean radius will be suggested, and then by employing initial distributions of the type given in Table I we shall describe how this process would yield rate curves similar to those found in Fig. 2.

If it is assumed that the initiation period is due to the presence of an inhibitor in the absence of a catalyst, this inhibitor is distributed between the water and styrene so that the system is in equilibrium. As soon as the catalyst (which in general is much more soluble in water than in styrene) is added, it reacts with the inhibitor in the water, destroys its equilibrium between the two phases, and causes inhibitor to diffuse from the styrene into the water. If there exists a critical concentration of inhibitor in the styrene below which it polymerizes, it is clear that polymerization would start in a styrene globule as soon as enough inhibitor diffuses from it to reduce its inhibitor concentration to a value less than the critical. Since diffusion from a large globule is slower (as will be shown in the mathematical section of this paper) than from a small globule, the small globules in an emulsion would start to polymerize before the larger ones, and emulsions of small mean globule radius would polymerize faster than those of large mean globule radius provided that both have the same initial inhibitor concentration. This is in agreement with the rate curves in Fig. 2.

If initially a styrene-water emulsion has a sphere size distribution similar to one of those in

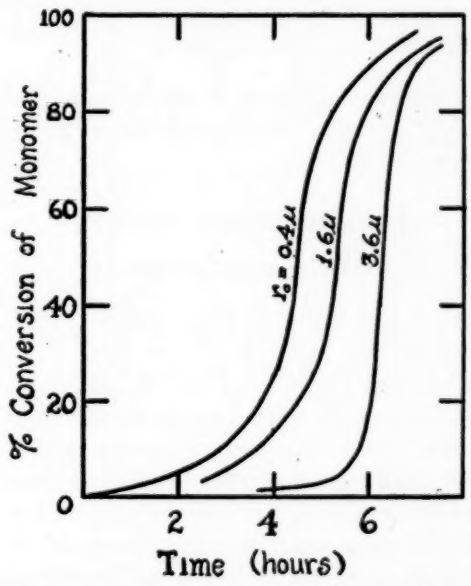

FIG. 2. Rate of polymerization of monostyrene for various initial mean globule radii when ammonium oleate is used as an emulsifier and sodium perborate as a catalyst.

Table I, according to our model, upon addition of catalyst the smaller globules start to polymerize first. Since there are initially relatively few small globules, the extent of polymerization changes very slowly at first. As time goes on the larger globules become available for polymerization as the result of two effects. First, more inhibitor diffuses out of them leaving them with inhibitor concentrations lower than the critical. Secondly, as the small globules polymerize, they give up their soap, thus increasing the emulsifier concentration and reducing the sizes of the

[4] This process is similar to that given by Mark, Hohenstein, and Siggia.

larger globules, causing them to polymerize sooner than they would otherwise.

One would expect both of these effects to contribute to an increasing polymerization rate until practically all the globules are able to start polymerizing, after which time there could be no increases in the rate. This process is in agreement with the individual rate curves in Fig. 2.

In the next part of this paper we shall make a detailed mathematical study of the processes described here. It will be divided into six sections:

I. Inhibition time.
II. Variation in mean radii with variation in soap concentration.
III. General reaction equation.
IV. Globule radius distribution functions.
V. Solution of reaction equation.
VI. Discussion of numerical results.

The effect of swelling of polymer by residual monomer on reaction rates is neglected in the following discussions.

B. MATHEMATICAL SECTION

I. Inhibition Time

One of the most striking properties of the polymerization rate curves in Fig. 2 is the initiation period which depends on the initial mean radius of the spheres in the dispersed phase. We have already suggested that this period in a particular globule is related to the time required for a certain amount of inhibitor to diffuse out of the globule of monomer. In order to apply this conjecture to a mathematical theory of the rate curves, we must give a definite description of the diffusion process. In particular we must derive a relation between the radius of a suspended monomer sphere and the time required for the sphere to achieve a state from which polymerization can start.

Let us suppose that at time $t=0$ a sphere of radius R of one liquid, L_0, is suspended in another liquid, L_e, and that at equilibrium c_0 is the concentration of a solute S in L_0 and c_e is the concentration of S in L_e. If to the L_e-L_0 system a reagent is added which reacts with the solute dissolved in L_e but not that dissolved in L_0, equilibrium is destroyed, and solute must diffuse into L_e until equilibrium is reestablished. Under the assumption that catalyst reacts with the solute S as soon as it diffuses into the water phase (i.e., $c_e=0$ if $t\geqslant 0$) we shall calculate the concentration of S at various points in the sphere L_0 as a function of time.

According to Fick's law, the concentration $c(r, t)$ of S at a point a distance r from the center of the sphere at time t is given by

$$D(\partial^2/\partial r^2)(rc)=(\partial/\partial t)(rc),$$

where D is the diffusion constant of S in L_0. If at time $t=0$ the sphere has a uniform solute concentration c_0, we have the initial conditions when

$$t=0, \quad r\leqslant R, \quad (rc)=rc_0,$$

and if there is infinite permeability at the L_0-L_e interface, we have the boundary conditions:

$$\text{when } t>0, \quad r=R, \quad (rc)=0; \quad r=0, \quad (rc)=0.$$

One can easily show that the solution of the diffusion equation under these conditions[5] is

$$c(r, t)=(2Rc_0/\pi r)\sum_{n=1}^{\infty}\frac{(-1)^{n+1}}{n}\sin(n\pi r/R)\times\exp-\{n^2\pi^2Dt/R^2\}.$$

If $C(t)$ is the average concentration at time t,

$$C(t)=(3/4\pi R^3)\int_0^R 4\pi r^2c(r, t)dr$$

$$=(6c_0/\pi)\sum_{n=1}^{\infty}(1/n^2)\exp-\{n^2\pi^2Dt/R^2\},$$

and as t increases only the first term becomes significant:

$$C(t)/c_0\simeq(6/\pi)\exp-\pi^2Dt/R^2.$$

So, the time required for the average concentration of a sphere of radius R to become $C(t)$ is

$$t\simeq(R^2/D^2)\log(6c_0/\pi C(t)). \qquad (1)$$

In our theory of emulsion polymerization we shall assume that there is a critical average concentration c^* which a globule must have before it polymerizes. Thus, a globule of radius R will not start to polymerize until the time t given by (1) when $C(t)=c^*$. Stated in another way, at

[5] W. Byerly, *Fourier Series* (Ginn and Company, New York, 1893), p. 116.

time t all spheres of radius less than

$$R \simeq t^{\frac{1}{2}}/\{(1/\pi^2 D) \log (6c_0/\pi c^*)\}^{\frac{1}{2}}, \quad (1a)$$

will be polymerizing. This expression can be written in a simpler form by introducing the time, τ, required for a sphere of unit radius to start polymerizing. In terms of τ, we have

$$R \simeq (t/\tau)^{\frac{1}{2}}. \quad (2)$$

There are many objections that could be raised in the manner in which (2) was obtained, but even under more exact treatment one finds that R is still roughly proportional to $t^{\frac{1}{2}}$.

II. Change in Sphere Diameter with Emulsifier Concentration

It has been observed experimentally that the mean radius of the suspended spheres in an emulsion decreases with increasing emulsifier concentration. In Fig. 1 we have plotted the mean sphere radius of a styrene emulsion in water as a function of emulsifier (ammonium oleate) concentration. The curve indicates that (except possibly in the range of very small radii) the mean radius varies linearly with the concentration, and can therefore be represented by the equation

$$(r-r_0)/(c-c_0) = (r_0-r_1)/(c_0-c_1), \quad (3)$$

where (r_0, c_0) and (r_1, c_1) are two points on the linear portion of the curve. In our analysis it will be assumed that the mean radius, r, is a linear function of the concentration over the entire concentration range.

From (3) it is possible to obtain a relation between mean radius and extent of reaction. We define the extent of reaction as

$$\alpha = [V(0) - V(t)]/V(0), \quad (4)$$

where $V(t)$ is the total volume of suspended spheres of monomer at time t (we assume that the spheres of monomer have a constant density independent of radius). Another convenient variable is

$$\beta = 1-\alpha. \quad (4a)$$

Suppose c_0 is the emulsifier concentration corresponding to the initial mean radius r_0 at the beginning of the reaction. Since in the reactions in which we are interested emulsifier is adsorbed on the monomer globule surfaces and is given up by the monomer as it is polymerized, the free soap concentration increases linearly with the loss in total surface of the monomer globules, thus

$$c = c_0 + c'(s(0) - s(t)),$$

where c' is a constant and $s(t)$ is the total surface of all the globules at time t. If $r_1 = 0$, c_1 is the emulsifier concentration when the reaction is completed (i.e., when $s(t) = 0$) or

$$c_1 = c_0 + c's(0).$$

Introducing these concentration relations into (3) we have

$$(r-r_0)/(s(0)-s(t))c' = -r_0/c's(0),$$

or

$$r = r_0 s(t)/s(0). \quad (4b)$$

Unfortunately the ratio $s(t)/s(0)$ is not a convenient quantity for later calculations; however, if the ratio $V(t)/V(0) = \beta$ could be used to approximate it, the equation

$$r \simeq r_0 \beta \quad (5)$$

would be useful in developing our reaction-rate theory.

When the reaction begins, $t = 0$ and

$$s(t)/s(0) = V(t)/V(0) = 1,$$

and when the reaction is completed

$$s(t) = V(t) = 0.$$

So (5) is exact in the two extremes $\beta = 1$ and $\beta = 0$. For the binomial and normal globule radius distributions that we shall use later, the agreement between the volume ratio and surface ratio turns out to be as good as necessary for the calculations in this paper. The largest percentage disagreement occurs in the range of small mean radii, where the assumption of a linear relation between soap concentration and mean globule radius is no longer valid anyhow. On the basis of these approximations our rate curves should be least accurate at the end of the polymerization process.

The error involved in the application of (5) is probably largest in the case of a sharp radius distribution. In fact, with a uniform radius distribution (all spheres with the same radius) we have

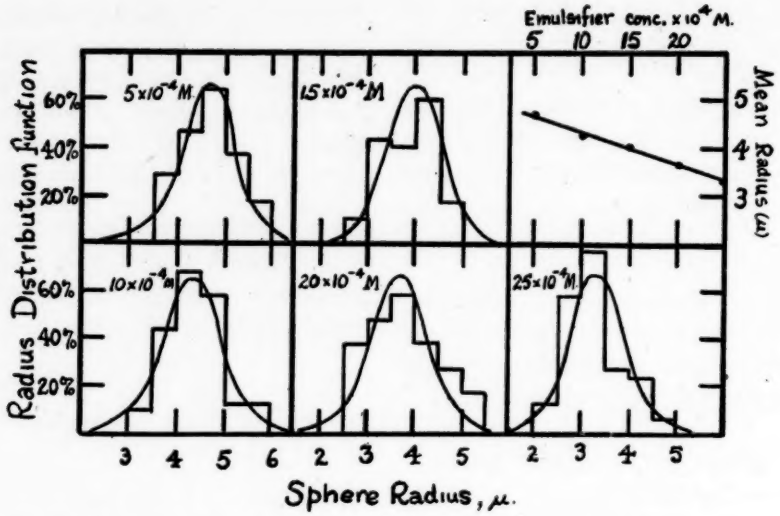

FIG. 3. Sphere size distributions for various emulsifier concentrations as taken from Clayton's data.

$$s(t)/s(0) = N(t)r^2/N(0)r_0^2,$$

and

$$\beta = V(t)/V(0) = r^3N(t)/r_0^3N(0),$$

where $N(t)$ is the total number of globules (all with radius r) at time t. Thus, in this case, combining the above two equations with (4b)

$$r = r_0\beta^{\frac{1}{3}}. \tag{5a}$$

In broader distributions the exponent on β is probable between $\frac{1}{2}$ and 1.

One immediate result of (5) and (5a) is that they allow one to express the mean radius of the monomer-polymer mixture as a function of the extent of the reaction, α. If we let

r_m = mean monomer radius,
r_p = mean polymer radius,

the mean radius of hydrocarbon spheres that would be observed experimentally is (using (5))

$$\begin{aligned}\langle r\rangle_{Av} &= r_m(1-\alpha)+\alpha r_p \\ &= r_0(1-\alpha)^2+\alpha r_p.\end{aligned} \tag{6}$$

A similar result can be obtained in the case of a homogeneous distribution from (5a),

$$\langle r\rangle_{Av} = r_0(1-\alpha)^{\frac{1}{3}}+\alpha r_p. \tag{6a}$$

If for all extents of reaction the mean radius of polymer globules is the same as their final mean radius after polymerization is completed, (6) and (6a) allow one to calculate $\langle r\rangle_{Av}$ from a knowledge of the initial and final mean radius of the globules. Early in the reaction this assumption is probably in error due to the swelling of polymer globules by monomer; however, r_p has α as a coefficient so that the mean radius is less sensitive to errors in r_p in this range.

III. General Reaction Equation

We shall now derive a differential equation for the extent of reaction under the assumptions that

a. Reaction takes place at boundary of suspended spheres,
b. Reaction rate is proportional to total surface area of suspended spheres,
c. No sphere begins to react until its average inhibitor concentration reaches a critical value, say c^*, and after that the reaction rate of a particular sphere is independent of the inhibitor concentration of that sphere.

As was shown in section I, at a time t all spheres of radius less than R are polymerizing if R is given by $R=(t/\tau)^{\frac{1}{3}}$, where τ is the time required for a sphere of unit radius to start polymerizing and is related to c^* by (1a) and (2).

TABLE II. Effect of emulsifier concentration on mean radius and standard deviation of sphere radius distribution function.

Soap conc., 10^4 M	5	10	15	20	25
Mean radius, $\bar{r}$, (microns)	4.67	4.36	4.01	3.65	3.27
Standard deviation, σ	0.587	0.600	0.672	0.620	0.587

If $G(r, t)dr$ is defined to be the number of monomer spheres of radius between r and $r+dr$ at time t, assumptions a–c and Eq. (2) imply that the rate at which the total volume of monomer is suspension changes at time t is

$$dV(t)/dt = -k\int_0^{(t/\tau)^{\frac{1}{2}}} 4\pi r^2 G(r, t)dr, \qquad (7)$$

where k is the rate constant for the reaction. Now suppose $N(t)$ is the total number of spheres in suspension at time t. Then the fraction of spheres with radii between r and $r+dr$ at time t is

$$g(r, t)dr = [G(r, t)/N(t)]dr.$$

Clearly,

$$N(t) = \int_0^\infty G(r, t)dr,$$

$$V(t) = \int_0^\infty (4/3)\pi r^3 G(r, t)dr = N(t)\int_0^\infty (4/3)\pi r^3 g(r, t)dr.$$

Since from (4) $V(t) = V(0)\beta$,

$$-(d\log\beta/dt)\int_0^\infty r^3 g(r, t)dr = 3k\int_0^{(t/\tau)^{\frac{1}{2}}} r^2 g(r, t)dr, \qquad (8)$$

and, given a sphere size distribution $g(r, t)$, one can calculate the extent of reaction at a given time from this equation. Of course $g(r, t)$ is a function of β, so (8) is really a differential-integral equation. For calculating purposes it is convenient to introduce two new parameters, T and λ defined by

$$T = 3kt, \quad \lambda = 3k\tau, \qquad (9)$$

which change (8) into

$$-(1/\beta)(d\beta/dT)\int_0^\infty r^3 g(r, t)dr = \int_0^{(t/\tau)^{\frac{1}{2}}} r^2 g(r, t)dr. \qquad (10)$$

Equation (10) can be considered to be the fundamental reaction rate equation for emulsion polymerization.

IV. Sphere Size Distribution

As was mentioned in the general discussion, the sphere radius distribution of a stable emulsion can be expected to have a single maximum provided the emulsion is well stirred. This was exemplified in Clayton's data in Table I. The distribution functions of Table I are plotted in Fig. 3, as are their approximations by normal curves; these normal curves seem to be good approximations to Clayton's data.

The decrease in mean radius with increasing emulsifier concentration is clear from Figs. 1 and 3. In Table II we give the mean radius and standard deviation of globule radii from the mean as obtained from Clayton's data. This table indicates that to within the accuracy expected in this work the mean radius, $\bar{r}$, is a linear function of the soap concentration and the standard deviation is almost independent of the soap concentration. In the distributions given in Table I, the mean value of σ is 0.613μ.

On the basis of the data given in Tables I and II we shall for our numerical work assume that initially the radii of monomer spheres are distributed normally or according to binomial approximations of normal distributions. Furthermore, we shall assume that the standard deviations from $\bar{r}$ of these distributions are constants in a given emulsion, independent of the soap concentration.

If $g(r, t)dr$ is the fraction of monomer spheres with radii between r and $r+dr$ at time t, a normal distribution of sphere radii can be expressed analytically by

$$g(r, t) = [1/\sigma(2\pi)^{\frac{1}{2}}]\exp -(r-\bar{r})^2/2\sigma^2, \qquad (11)$$

$\bar{r}$ being a function of the time and according to (5) expressed by

$$\bar{r} \simeq r_0(1-\alpha) = r_0\beta,$$

where α is the extent of reaction a time t after catalyst has been added to a monostyrene emulsion with an initial mean sphere radius r_0. The simplest binomial approximation to a normal distribution is a rectangular distribution with the same mean radius and standard deviation. Analytically this can be written:

$$g(r, t) = \begin{cases} 0 & \text{if } |r-\bar{r}| > \sigma 3^{\frac{1}{2}} \\ 1/(2\sigma 3^{\frac{1}{2}}) & \text{if } |r-\bar{r}| \leqslant \sigma 3^{\frac{1}{2}}. \end{cases} \qquad (12)$$

A more complicated but more accurate binomial approximation to a normal function is the three rectangle approximation which can be represented analytically by

$$g(r,t)=\begin{cases}0 & \text{if } (r-\bar{r})>3\delta/2\\ 1(1/4\delta) & \text{if } 3\delta/2\geqslant(r-\bar{r})>\delta/2\\ 2(1/4\delta) & \text{if } \delta/2\geqslant(r-\bar{r})>-\delta/2\\ 1(1/4\delta) & \text{if } -\delta/2\geqslant(r-\bar{r})>3\delta/2\\ 0 & \text{if } -3\delta/2\geqslant(r-\bar{r}),\end{cases} \tag{13}$$

where

$$\delta=4\sigma(3/7)^{\frac{1}{2}}.$$

By taking more and more rectangles one can obtain increasingly more accurate binomial approximations.

V. Solution of the Reaction Equation

In this section we shall solve the reaction equation for several initial globule distributions. The physical nature of the solutions will be discussed in Section VI. Let us first consider the case of no initiation time. This might be applicable to situations where inhibitor is initially on the surface of the hydrocarbon globules but not in their interiors.

Whether there is an inhibitor or not in the globules, one must, in order to solve the reaction Eq. (10) evaluate

$$\langle r^3\rangle=\int_0^\infty r^3g(r,t)dr.$$

This we shall do in three cases.

(a) Rectangular Distribution. Application of (12) yields

$$\langle r^3\rangle=\int_{\bar{r}-\sigma3^{\frac{1}{2}}}^{\bar{r}+\sigma3^{\frac{1}{2}}}r^3(1/2\sigma3^{\frac{1}{2}})dr$$
$$=(1/8\sigma3^{\frac{1}{2}})\{(\bar{r}+\sigma3^{\frac{1}{2}})^4-(\bar{r}-\sigma3^{\frac{1}{2}})^4\}$$
$$=\bar{r}(\bar{r}^2+3\sigma^2).$$

(b) Binomial Distribution. ($\delta=2\sigma(3/7)^{\frac{1}{2}}$). Application of (13) yields

$$\langle r^3\rangle=\int_{\bar{r}+\delta/2}^{\bar{r}+3\delta/2}(r^3/4\delta)dr+2\int_{\bar{r}-\delta/2}^{\bar{r}+\delta/2}(r^3/4\delta)dr+\int_{\bar{r}-3\delta/2}^{\bar{r}-\delta/2}(r^3/4\delta)dr$$
$$=\bar{r}(\bar{r}^2+3\sigma^2).$$

(c) Normal Distribution.

$$\langle r^3\rangle=\int_{-\infty}^{\infty}[r^3/\sigma(2\pi)^{\frac{1}{2}}]\exp-(r-\bar{r})^2/2\sigma^2dr$$
$$=\bar{r}(\bar{r}^2+3\sigma^2).$$

It is to be noted that in all three cases (and indeed for any binomial distribution)

$$\langle r^3\rangle=\bar{r}(\bar{r}^2+3\sigma^2). \tag{14}$$

With no initiation period we must use

$$\langle r^2\rangle=\int_0^\infty r^2g(r,t)dr=\bar{r}^2+\sigma^2. \tag{15}$$

With (14) and (15) one can solve (10).

1. *No Initiation Period*

When there is no initiation period, (10) becomes, upon application of (14) and (15):

$$-(\bar{r}/\beta)(d\beta/dT)(\bar{r}^2+3\sigma^2)=(\sigma^2+\bar{r}^2),$$

a result valid for all binomial distributions. Since $\bar{r}=\beta r_0$,

$$-r_0d\beta\left\{\frac{\beta^2+3(\sigma/r_0)^2}{\beta^2+(\sigma/r_0)^2}\right\}=dT. \tag{16}$$

Since at time $t=0$ (i.e., $T=0$) no polymerization has occurred, $\beta=1$, and the solution of (16) is

$$T=\alpha r_0+2\sigma(\tan^{-1}r_0/\sigma-\tan^{-1}\beta r_0/\sigma). \tag{17}$$

This equation is plotted in Figs. 4 and 5 for several values of r_0 and σ.

2. *Homogeneous Distribution with Inhibitor*

In the presence of an inhibitor the initial radius distribution easiest to treat is a homogeneous one. From the discussion in Section III, $\beta=1$ in this case until the time corresponding to

$$T=T_0=\lambda r_0^2,$$

where r_0 is the initial radius of all the hydrocarbon globules. After the time T_0, β is the solution of the differential equation obtained by introducing (5a) into (10) and choosing

$$g(r,t)=\begin{cases}1 & \text{if } r=r_0\beta^{\frac{1}{2}}\\ 0 & \text{otherwise:}\end{cases}$$

$$-(1/\beta)(d\beta/dT)(r_0\beta^{\frac{1}{2}})^3=(r_0\beta^{\frac{1}{2}})^2$$

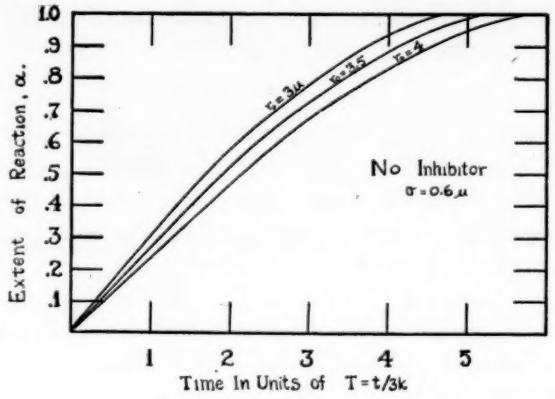

FIG. 4. Theoretical polymerization rate curves in the absence of inhibitor. Standard deviation of sphere radii from mean 0.6μ.

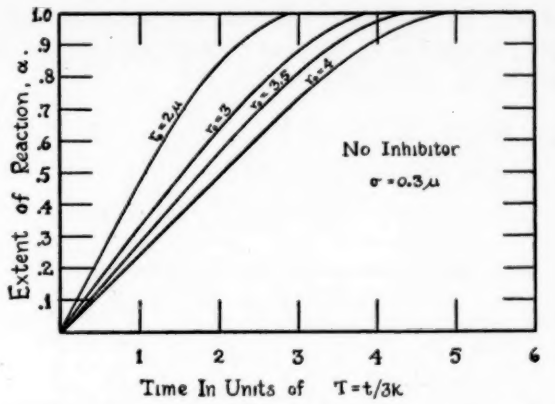

FIG. 5. Theoretical polymerization rate curves in the absence of inhibitor. Standard deviation of sphere radii from mean 0.3μ.

or

$$-r_0 d\beta/\beta^{\frac{1}{3}} = dT.$$

The solution of the equation is (employing the boundary condition $\beta=1$ when $T=T_0=\lambda r_0^2$)

$$1-\alpha=\beta=[1-(1/2r_0)(T-\lambda r_0^2)]^2. \quad (17a)$$

This equation is plotted in Fig. 6 for several values of r_0 when $\lambda=1$. It is to be noticed that the reaction starts suddenly at the end of the initiation time instead of gradually as one observes experimentally. By assuming a sphere size distribution of the type discussed in Section IV, one obtains theoretically the observed gradual increase in reaction rate at early times.

3. *Rectangular Distribution with Inhibitor*

The number of globules being polymerized at a given time in this case depends on the time. Since there are initially no globules of radius less than $(r_0-\sigma 3^{\frac{1}{2}})$, there can be no polymerization at times less than those corresponding to $T_0/\lambda=(r_0-\sigma 3^{\frac{1}{2}})^2$. For values of T/λ between T_0/λ and $T_1/\lambda=(r_0\beta_1\pm\sigma 3^{\frac{1}{2}})^2$ only part of the globules polymerize. Finally for times $>T_1/\lambda$ all globules have a sufficiently low inhibitor concentration for polymerization to take place. During each of these three time intervals the differential Eq. (10),

$$r_0(d\beta/dT)(r_0^2\beta^2+3\sigma^2) = -\int_0^{(T/\lambda)^{\frac{1}{2}}} r^2 g(r)dr,$$

has a different form. Applying (12),

(a) When $T\leqslant T_0$, $d\beta/dT=0$; (18a)

(b) When $T_0<T\leqslant T_1$,

$$r_0(d\beta/dT)(r_0^2\beta^2+3\sigma^2) = -\frac{1}{2\sigma 3^{\frac{1}{2}}}\int_{\beta r_0-\sigma(3)^{\frac{1}{2}}}^{(T/\lambda)^{\frac{1}{2}}} r^2 dr,$$

or

$$r_0(d\beta/dT)(r_0^2\beta^2+3\sigma^2) = -\frac{1}{6\sigma 3^{\frac{1}{2}}}[(T/\lambda)^{\frac{1}{2}}-(r_0\beta-\sigma 3^{\frac{1}{2}})^3]; \quad (18b)$$

(c) When $T>T_1$,

$$r_0(d\beta/dT)(r_0^2\beta^2+3\sigma^2) = -(r_0^2\beta^2+\sigma^2). \quad (18c)$$

Thus in each time interval the form of the solution of (18) is different. These solutions are to be combined through the boundary conditions at the beginning and end of each interval.

Interval (*a*). $T/\lambda\leqslant T_0/\lambda$. The solution of (18a) is $\beta=$constant. To fit the boundary condition of no polymerization at $t=0$, the constant must be 1, so for

$$T/\lambda\leqslant T_0/\lambda, \quad \beta=1. \quad (19a)$$

Interval (*b*). $T_0\leqslant T<T_1$. In this interval the solution of the differential Eq. (18b) is rather complicated. We shall assume that

$$\beta(T)=1+\sum_{n=1}^{\infty} a_n(T-T_0)^n/n!. \quad (19b)$$

According to Taylor's theorem,

$$a_n=d^n\beta(T_0)/dT^n.$$

If we let $\mu_3=r_0(r_0^2+3\sigma^2)$ and remember that $\beta=1$ when $T=T_0$, we find by successive differentiation of (18b) that

$$a_1=d\beta/dT]_{T=T_0}=0,$$
$$a_2=-T_0^{\frac{1}{2}}/[4\sigma\lambda\mu_3(3\lambda)^{\frac{1}{2}}],$$
$$a_3=-\{(T_0^{\frac{1}{2}}/4\lambda^{\frac{1}{2}})-a_2r_0(T_0/\lambda)\}/2\sigma\mu_3 3^{\frac{1}{2}}.$$

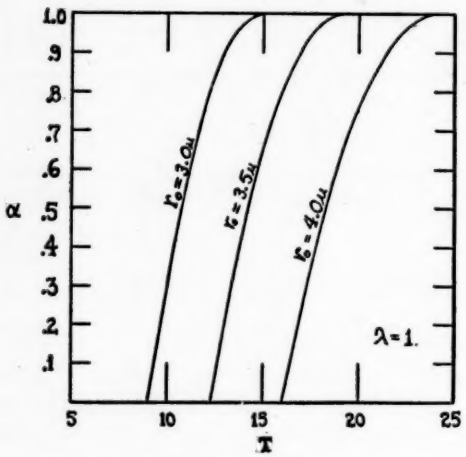

FIG. 6. Theoretical variation of degree of polymerization, α, with time.

For reasonable values of r_0, T_0, λ, and σ the main contribution (over 90 percent) of a_3 comes from the term proportional to a_2, and in general, the dominant term in a_n is proportional to a_{n-1}, so that

$$a_n\simeq a_{n-1}r_0(T_0/\lambda)/(2\sigma\mu_3 3^{\frac{1}{2}}).$$

Application of this approximation to (19a) yields

$$\beta-1\simeq-\{\sigma\mu_3(3\lambda)^{\frac{1}{2}}/r_0^2T_0^{\frac{1}{2}}\}\times\{\exp(T-T_0)(r_0T_0/2\sigma\lambda\mu_3 3^{\frac{1}{2}})-1-(T-T_0)r_0T_0/2\sigma\mu_3\lambda 3^{\frac{1}{2}}+O(T-T_0)^3\}.$$

The correction terms of $O(T-T_0)^3$ can be written as a power series in $(T-T_0)$ (starting with $(T-T_0)^3$). Numerically they are small compared with the first three terms in the above equation; however, for completeness we shall include several of them in the final expression:

$$-\alpha=\beta-1=-\{\sigma\mu_3(3\lambda)^{\frac{1}{2}}/r_0^2T_0^{\frac{1}{2}}\}\times\{\exp(T-T_0)(r_0T_0/2\sigma\lambda\mu_3 3^{\frac{1}{2}})-1-(T-T_0)T_0r_0/2\sigma\lambda\mu_3 3^{\frac{1}{2}}+T_0r_0^2(T-T_0)^3/144\sigma^2\mu_3^2\lambda^2+[2r_0^3T_0^2(3T_0\lambda)^{\frac{1}{2}}/\sigma\lambda^2\mu_3^2-1]r_0^2\times(T-T_0)^4/1152\sigma^2\lambda^2\mu_3^2+\cdots\}. \quad (20)$$

This expression is valid until T becomes sufficiently large so that

$$T=\lambda[r_0\beta+\sigma(3)^{\frac{1}{2}}]^2. \quad (21)$$

For larger values of T, (18b) is no longer valid, and (20) does not apply. If we define T_1 and β_1 as the values of T and β for which (20) and (21) are satisfied simultaneously, we have as boundary conditions for (18c) $T=T_1$ when $\beta=\beta_1$.

Interval (c). $T>T_1$. In this interval one can easily obtain a closed relation between T and β by solving (18c) with the above boundary conditions. Thus

$$(T_1-T)=r_0(\beta-\beta_1)+2\sigma(\tan^{-1}\beta r_0/\sigma-\tan^{-1}\beta_1 r_0/\sigma). \quad (22)$$

The complete solution of (10) for all times is the combination of the solutions in intervals *a*, *b*, and *c*. This solution is plotted in Figs. 7–8 for several values of r_0, σ, and λ. It will be discussed in detail in Section VI.

4. *Binomial Distribution with Inhibitor*

In the binomial distribution (11) there is initially no globule of radius less than $r_0-(3\delta/2)$ (where $\delta=4\sigma(3/7)^{\frac{1}{2}}$) so there cannot be any polymerization until times corresponding to $T_0=\lambda(r_0-3\delta/2)^2$. With this distribution we must consider separately five time intervals in each of which (10) takes on a different form. Whenever $g(r,t)$ changes its form a new interval begins. If these intervals begin at times corresponding to T_0, T_1, T_2, ... we shall let the values of β at these times be 1, β_1, β_2, ... The five required differential equations with their boundary conditions are:

(a) When $T<T_0=\lambda(r_0-3\delta/2)^2$,

$$d\beta/dt=0 \quad (23a)$$

with the boundary condition $\beta=1$ when $T=0$.

(b) When $\beta r_0-3\delta/2<(T/\lambda)^{\frac{1}{2}}<\beta r_0-\delta/2$,

$$r_0(d\beta/dT)(r_0^2\beta^2+3\sigma^2)=(-1/12\delta)\{(T/\lambda)^{\frac{1}{2}}-(r_0\beta-3\delta/2)^3\} \quad (23b)$$

with boundary condition $\beta=1$ when $T=T_0=\lambda(r_0-3\delta/2)^2$.

(c) When $\beta r_0-\delta/2<(T/\lambda)^{\frac{1}{2}}<r_0\beta+\delta/2$,

$$r_0(r_0^2\beta^2+3\sigma^2)d\beta/dT=-(1/12\delta)\{2(T/\lambda)^{\frac{1}{2}}-(\beta r_0-\delta/2)^3-(\beta r_0-3\delta/2)^3\} \quad (23c)$$

with the boundary conditions $\beta=\beta_1$ when $T=T_1=\lambda(r_0\beta_1-\delta/2)^2$.

(d) When $\beta r_0+\frac{1}{2}\delta<(T/\lambda)^{\frac{1}{2}}<\beta r_0+3\delta/2$,

$$r_0(\beta^2r_0^2+3\sigma^2)d\beta/dT = -(1/12\delta)\{(T/\lambda)^{\frac{1}{2}}+(r_0\beta+\tfrac{1}{2}\delta)^3 - (r_0\beta-\tfrac{1}{2}\delta)^3-(r_0\beta-3\delta/2)^3\} \quad (23d)$$

with the boundary condition $\beta=\beta_2$ when $T=T_2=\lambda(\beta_2r_0+\frac{1}{2}\delta)^2$.

(e) When $(T/\lambda)^{\frac{1}{2}}>\beta r_0+3\delta/2$,

$$r_0(r_0^2\beta^2+3\sigma^2)(d\beta/dT)=-(r_0^2\beta^2+\sigma^2) \quad (23e)$$

with the boundary condition $\beta=\beta_3$ when $T=T_3=\lambda(\beta_3r_0+3\delta/2)^2$.

In the interval (a), as in the case of a rectangular distribution, $\beta=1$ when $T<T_0$. In interval (b) we proceed in the same manner as in the rectangular distribution and obtain:

$$-\alpha=\beta-1=-\frac{2\delta\mu_3(\lambda/T_0)^{\frac{1}{2}}}{r_0^2T_0}\left\{\exp\left[\frac{T_0(T-T_0)}{4\delta\lambda(r_0^2+3\sigma^2)}\right] -1-\frac{T_0(T-T_0)}{4\delta\lambda(r_0^2+3\sigma^2)}+O(T-T_0)^3\right\}. \quad (24a)$$

In interval (c):

$$\beta=\beta_1+a_1(T-T_1)+a_2(T-T_1)^2/2!+\cdots \quad (24a)$$

where

$$a_1=-\frac{1}{12r_0}\left(\frac{3(T_1/\lambda)-3\delta(T_1/\lambda)^{\frac{1}{2}}+\delta^2}{r_0^2\beta_1^2+3\sigma^2}\right), \text{ etc.,} \quad (24b)$$

each a_i being obtained by taking successive derivatives of (23c). In interval (d):

$$\beta=\beta_2+a_1(T-T_2)+a_2(T-T_2)^2/2!+\cdots \quad (24c)$$

where

$$a_1=-\frac{1}{4r_0}\left(\frac{3(T_2/\lambda)-5\delta(T_2/\lambda)^{\frac{1}{2}}+3\delta^2}{r_0^2\beta_2^2+3\sigma^2}\right), \text{ etc.}$$

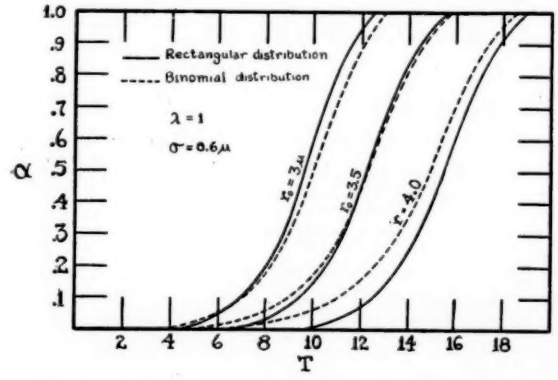

FIG. 7. Theoretical polymerization rate curves with inhibitor.

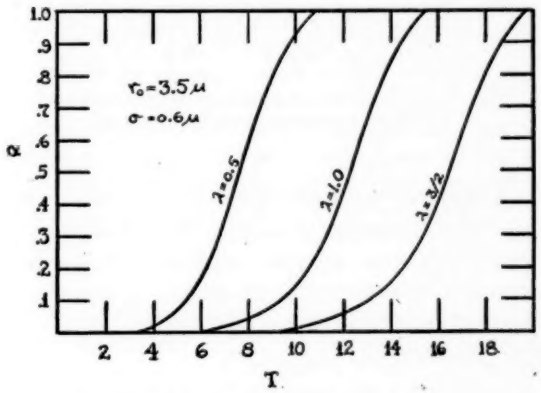

FIG. 8. Theoretical polymerization rate curves at constant initial inhibitor concentration, standard deviation, and mean radius.

In interval (e):

$$(T-T_3)=r_0(\beta-\beta_3)+2\sigma(\tan^{-1}\beta r_0/\sigma - \tan^{-1}\beta_3r_0/\sigma). \quad (24d)$$

The complete curve of α as a function of time as obtained by combining the above equations is plotted in Fig. 7.

In the case of a normal distribution Eq. (10) cannot be solved directly by quadratures, but any of the well known methods of numerical integration of first-order differential equations can be applied. The results are similar to those we have obtained from binomial distributions.

VI. Discussion of Numerical Results

Equation (17) of the last section gives the extent of reaction, α, as a function of time when (a) no inhibitor is present, and, (b) the initial monomer distribution is binomial. From (17) it is clear that the dependence of α on time is determined by two parameters, r_0, the initial mean radius of the monomer globules, and σ, the standard deviation of their radius distribution. Figures 4 and 5 show that under conditions (a) and (b) polymerization starts immediately, and

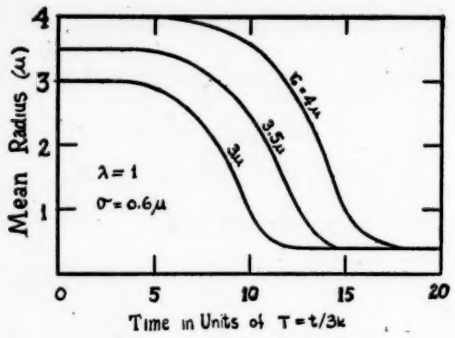

FIG. 9. Theoretical variation with time of mean radius of monomer-polymer mixture.

of all systems with the same initial mean radii, those of the smaller standard deviation (that is, those with the sharper radius distributions) polymerize faster. Of all those of the same standard deviation those with the smaller mean radii polymerize faster.

Equations have been derived for the progress of the polymerization reaction when inhibitor is present for two initial sphere radius distributions: (*a*) rectangular distribution, and (*b*) binomial distribution. In case (*a*), α is given as a function of time in Eqs. (19), (21), and (22) while the results for case (*b*) are given in (24a)–(24d). Besides the parameters r_0 and σ, one more parameter λ, a measure of the time required for inhibitor to diffuse out of a monomer sphere of unit radius, is needed to completely describe the variation of α with time. α is plotted in Fig. 7 as a function of time for several initial mean radii when $\lambda=1$ and $\sigma=0.6$. It is to be noted that, except for very early times, the rate curves of distributions (*a*) and (*b*) corresponding to the same initial mean radii are very similar. Indeed, the detailed shape of the initial distribution is not nearly as important as its standard deviation and mean radius in determining the character of the extent of reaction curves. The curves in Fig. 7 resemble closely the experimental curves of Fig. 2 in the manner in which they exhibit the increase in the initiation period that occurs when the initial mean radius is increased. In Fig. 8 the extent of reaction is plotted for several values of λ while σ and r_0 are kept fixed. The larger the value of λ the longer the inhibition period.

In Fig. 9 the mean radius of the polymer-monomer mixture is plotted as a function of time using Eq. (6) and the curves corresponding to the binomial distribution in Fig. 7.

In conclusion the author wishes to thank Professor H. Mark and Dr. W. P. Hohenstein, who have been doing experimental work on emulsion polymerization, for suggesting this problem and for their helpful advice during its investigation.

Letters to the Editor

THIS section will accept reports of new work, provided these are terse and contain few figures, and especially few halftone cuts. The Editorial Board will not hold itself responsible for opinions expressed by the correspondents. Contributions to this section should not exceed 600 words in length and must reach the office of the Managing Editor not later than the 15th of the month preceding that of the issue in which the letter is to appear. No proof will be sent to the authors. The usual publication charge ($3.00 per page) will not be made and no reprints will be furnished free.

Molecular Constants and Chemical Theories

W. F. LUDER
Northeastern University, Boston, Massachusetts
July 9, 1945

IT seems obvious that the interesting controversy between R. Samuel and C. W. Wheland[1] cannot be settled by appeals to wave mechanics. But citation of a few experimental facts will show that the extreme position for and against the octet theory cannot be maintained by either.

Samuel's reaction against the octet theory is justified, but cannot be supported by discarding the coordinate bond. Wheland's reaction against abandoning the coordinate bond is justified, but cannot be supported by maintaining the octet theory. The "octet theory" must be abandoned, but the coordinate bond cannot be given up.

The existence of the chemistry of addition compounds (not mentioned by either Samuel or Wheland) requires the concept of the coordinate bond, e.g., in the reaction between BCl_3 and NH_3. On the other hand, the existence of a large number of "violations" of the octet rule requires *its* abandonment. Covalent compounds such as PF_5, SF_6, IF_7, and OsF_8 show that the octet rule is rigorously valid only for the second period of the periodic table from Li to Ne. This is admitted by Dr. Wheland in a footnote.

[1] J. Chem. Phys. 13, 239 and 251 (1945).

Solute Type and Viscosity of Dilute Solutions of High Polymers

RUDOLPH SPEISER AND R. T. WHITTENBERGER
Eastern Regional Research Laboratory, Philadelphia 18, Pennsylvania[1]
July 2, 1945

FRITH[2,3] has recently considered the theoretical significance of the slope of $\eta_{sp}/c-c$ curves for solutions of high polymers. By statistical and quasithermodynamical analysis, she has shown that the slope is related to the energy of polymer-solvent interaction, the slope being greater for a good solvent or solvent mixture than for a poor one.[3,4] Frith has also shown that at low concentrations her equation for the variation of η_{sp}/c with c is similar to Huggins'.[5]

In Huggins' equation the slope, $k'[\eta]^2$, is proportional to the square of the intrinsic viscosity, and the constant, k', is characteristic, and independent[4,5] of the intrinsic viscosity for a given polymer-solvent system. This invariance of k' makes it a more useful quantity for discussion than the slope. For this reason we have combined Frith's and Huggins' equations to obtain the following relation among the constants:

$$k'=B'/[\eta]^2-Bw/[\eta]^2kT=A-B''w/T. \qquad (1)$$

where A and B'' are independent of $[\eta]$.

The second term accounts for the variation of η_{sp}/c with concentration due to the energy of interaction, w, between the polymer chain segment and solvent molecules, whereas the first term accounts for variations with concentration due to other causes, such as differing internal structure. w is negative[2] when a tendency exists for solvation of the polymer chain segment. Thus, if a solvent is made inferior by addition of a non-solvent, which leads to a less negative w, k' decreases; if a better solvent is used, w has a more negative value and k' increases. Likewise, if the energy of interaction is constant and only the internal structure is changed, k' varies with A.

Variations of k' can be divided into two cases: (1) the interaction energy, w, remains constant and A varies; (2) A remains constant and w varies by changing (a) the

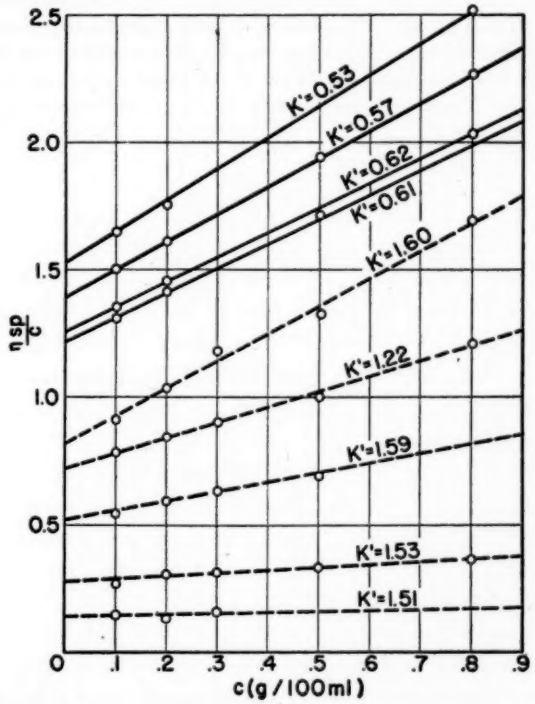

FIG. 1. $\eta_{sp}/c-c$ curves for potato amylose and amylopectin fractions in 2 percent KOH. Solid lines amylose. Dashed lines amylopectin. Amylose and amylopectin were separated from whole starch with nitrobenzene. (See reference 8.) Amylose components (and amylopectin components) were fractionally precipitated by isopropyl alcohol from 0.5 percent KOH.

TABLE I.—k' values calculated from $\eta_{sp}/c - c$ curves for pectin nitrate-acetone solutions.

Treatment of pectin sample before nitration	Degree[b] of methyl esterification	k'	N
Untreated	0.75[c]	$0.87 \pm .02$[d]	9.4%
Acid deesterified[a]	0.24[c]	$0.19 \pm .02$[d]	9.4

[a] For method, see C. H. Hills, J. W. White, Jr., and G. L. Baker, Proc. Inst. Food Tech. page 47 (1942).
[b] $\lambda = [COOCH_3]/([COOH] + [COOCH_3])$; C. H. Hills and R. Speiser, Science, in press.
[c] Degree of methyl esterification before nitration. Nitration results in approximately 30 percent methyl deesterification.
[d] Average for five fractions of different intrinsic viscosity.

solvent or (b) the solute type. Case 2(b) is often trivial but becomes important when one studies the change in polymer-solvent interaction as the nature of the surface of the molecule is changed.

Numerous examples of Case 2(a) may be found in the literature.[2,4,5] A possible example of Case 1 was the observation of Bartovics and Mark[6] on polystyrene that k' changes with the temperature of polymerization. This variation in k' was attributed to a change in the internal structure of the polystyrene as a result of a change in the mechanism of polymerization with the temperature.

We have obtained viscosity data which provide good examples of Cases 1 and 2(b). Figure 1 represents $\eta_{sp}/c - c$ curves for fractionated potato amylose and amylopectin (Case 1). It is evident that k' (computed from Huggins' equation) for amylose (linear chain) and amylopectin (branched chain) fractions, respectively, is independent of the intrinsic viscosity. However, $k' = 0.58 \pm 0.02$ for amylose[7] is considerably less than $k' = 1.49 \pm 0.10$ for amylopectin. These two substances have a well-recognized difference in molecular structure. Since both amylose and amylopectin are composed of glucose residues, w for amylose and amylopectin must be nearly identical, and the difference in k' must be due to a difference in A for the two molecules. These results suggest that this method may provide a means of detecting branching in high polymers.

Case 2(b) is illustrated by pectin nitrate solutions in acetone for which Table I lists average values of k' for five fractions. Two samples were used, their degree of methyl esterification before nitration being 0.75 and 0.24. The k's for the pectin nitrate fractions obtained from ea sample are independent of the intrinsic viscosity, but k for "high ester" pectin nitrate is greater than that for "low ester" pectin nitrate. In this example, the solu molecule is principally altered through replacement of methyl ester groups by carboxyls, thus changing polymer-solvent interaction, with consequent variation of k'. Because methyl ester groups are more compatible with acetone than carboxyl groups, k' for pectin nitrate made from the untreated pectin is greater than k' for the acid deesterified pectin nitrate.

[1] One of the laboratories of the Bureau of Agricultural and Industrial Chemistry, Agricultural Research Administration, United States Department of Agriculture.
[2] E. M. Frith, Trans. Faraday Soc. **41**, 17, 90 (1945).
[3] E. M. Frith and R. F. Tuckett, Nature **155**, 164 (1945).
[4] T. Alfrey, A. Bartovics, and H. Mark, J. Am. Chem. Soc. **64**, 1557 (1942).
[5] M. L. Huggins, J. Am. Chem. Soc. **64**, 2716 (1942).
[6] A. Bartovics and H. Mark, J. Am. Chem. Soc. **65**, 1901 (1943).
[7] Data of J. F. Foster and R. M. Hixon, J. Am. Chem. Soc. **65**, 618 (1943), yield $k' = 0.62$, 0.67, 0.57, and 0.65 for whole potato amylose, whole tapioca amylose, whole lily bulb amylose, and whole corn amylose, respectively. This agreement with our data for amylose is noteworthy, since Foster and Hixon's solvent was anhydrous ethylene diamine, whereas we used 2 percent KOH.
[8] R. L. Whistler and G. E. Hilbert, "Theory of the Fractionation of Starch. Separation of Amylose and Amylopectin by Means of Some Nitroparaffins." Unpublished manuscript at the Northern Regional Research Laboratory.